REVIEW
SPACE PHYSICS: IONOSPHERIC PHYSICS

Earth and Planetary Physics
9: 81–100, 2025
doi: 10.26464/epp2024074

Thermospheric neutral wind studies over the equatorial region: A review

Siti Syazwani Nasuha[1], Idahwati Sarudin[1*], Nurul Shazana Abdul Hamid[2,3*], and Ahmad Fairuz Omar[1]

[1]School of Physics, Universiti Sains Malaysia, 11800 USM, Pulau Pinang, Malaysia;

[2]Department of Applied Physics, Faculty of Science and Technology, Universiti Kebangsaan Malaysia, 43600 UKM Bangi, Selangor, Malaysia;

[3]Space Science Centre (ANGKASA), Institute of Climate Changes, Universiti Kebangsaan Malaysia, 43600 UKM Bangi, Selangor, Malaysia

Key Points:

- Thermospheric neutral winds (TNW) significantly influence the dynamics of the thermosphere–ionosphere system (TIS), but knowledge gaps remain in the finer understanding of their behavior and impacts due to limited monitoring and characterization efforts.
- The low-latitude equatorial region, particularly near the dip equator, exhibits unique interactions with TNW modulated by the Earth's magnetic field lines, which necessitates more focused investigations regarding the relevant parameters to further understand these complexities.
- An integrated approach combining empirical observations, first-principles methods, and advanced numerical models is necessary to accurately characterize TNW in equatorial regions, enhancing our ability to improve atmospheric models, predict global dynamics, and refine space weather forecasting.

Citation: Nasuha, S. S., Sarudin, I., Hamid, N. S. A., and Omar, A. F. (2025). Thermospheric neutral wind studies over the equatorial region: A review. *Earth Planet. Phys.*, *9*(1), 81–100. http://doi.org/10.26464/epp2024074

Abstract: Thermospheric neutral winds (TNWs) refer to the neutral gases in the thermosphere circulating as tides, which play a crucial role in the dynamics of the thermosphere–ionosphere system (TIS). Global geospace neutral winds, particularly over the magnetic equator, have been a subject of study for several decades. However, despite the known importance of neutral winds, a comprehensive understanding and characterization of the winds is still lacking. Various ground-based and satellite missions have provided valuable information on the contribution of neutral winds to the global atmospheric dynamics. However, efforts in the global monitoring of neutral winds are still lacking, and the drivers behind the behavior of TNWs as well as their influence on the TIS remain incomplete. To address these knowledge gaps in the global circulation of TNWs, it is crucial to develop a deep understanding of the neutral wind characteristics over different regions. The low-latitude equatorial region in particular has been observed to exert complex influences on TNWs because of the unique effects of the Earth's magnetic field at the dip equator. Studying neutral winds over this region will provide valuable insights into the unique dynamics and processes that occur in this region, thereby enhancing our understanding of their role in the overall dynamics of the TIS. Additionally, through empirical observations, an improved ability to accurately model and predict the behavior of this region can be achieved. This review article addresses challenges in understanding equatorial winds by reviewing historical measurements, current missions, and the interactions of ionospheric and thermospheric phenomena, emphasizing the need for comprehensive measurements to improve global atmospheric dynamics and weather forecasting.

Keywords: thermospheric neutral wind; thermosphere–ionosphere system; dip equator; equatorial region

1. Introduction

The Earth's atmosphere is a complex layer of gases structured into several distinct zones based on temperature and composition. It is typically differentiated into two parts: the lower atmosphere, consisting of the troposphere and stratosphere, and the upper atmosphere, which includes the mesosphere, thermosphere, ionosphere, and exosphere (Laštovička, 2023). The thermosphere extends from approximately 85 to 550 km above the Earth's surface (Dhadly et al., 2023). Its upper boundary merges with the non-Maxwellian exosphere, whereas its lower boundary separates it from the mesosphere at the mesopause. Overlapping with the mesosphere and thermosphere is the ionosphere, which is a partially ionized region within Earth's upper atmosphere that is characterized by a high concentration of ions and free electrons. The thermosphere differs from other layers of the upper atmosphere because of its composition of light gases, such as atomic oxygen, molecular nitrogen, and helium (Solomon and Roble, 2015). However, because of its high altitude, the density of molecules in the thermosphere is extremely low, which means

First author: S. S. Nasuha, sitisyazwaninasuha@gmail.com
Correspondence to: I. Sarudin, idahwati@usm.my
N. S. A. Hamid, zana@ukm.edu.my
Received 15 MAY 2024; Accepted 25 OCT 2024.
First Published online 05 DEC 2024.

that collisions between neutral particles are relatively infrequent. This situation leads to altitudinal differentiation of the thermospheric composition as the gases become separated based on chemical and physical processes. For example, solar radiation in the far ultraviolet dissociates molecular oxygen at altitudes near 130 km into atomic oxygen, which moves downward (through molecular diffusion and other transport) to heights around 95 km, where sufficient collisions occur and three-body recombination recombines it into molecular oxygen and ozone (Burns et al., 2021). Overall, the low to middle thermosphere (~100–300 km) is characterized by the presence of heavier gases, such as molecular nitrogen and oxygen, whereas the upper thermosphere (up to ~550 km) is more abundant in atomic oxygen.

The thermosphere makes up a large part of the upper atmosphere system; hence, any slight variations caused by external energy input may result in direct changes observed at other altitudes. These changes may be reflected in the mesosphere, lower thermosphere, and ionosphere through the distribution of heat, momentum, and energy carried out by neutral winds in the thermosphere. As identified by Rishbeth (1972), the thermospheric neutral winds (TNWs) are mainly driven by (1) pressure gradients resulting from solar heating; (2) frictional forces attributable to the viscosity of the air; (3) ion drag from collision between ions and neutral particles; and (4) the Coriolis force, which arises from the rotation of the Earth. Throughout the 24-h day, TNW movement follows a predictable pattern mostly influenced by the global pressure gradient; however, an increase in solar activity may disrupt this behavior. Thermospheric neutral winds contribute to the overall circulation patterns of the Earth's atmosphere. Understanding TNWs helps elucidate the dynamics of the upper atmosphere and its coupling with lower atmospheric layers so that subsequently, we can improve existing models and predictions of upper atmospheric weather and dynamics.

The neutral winds in the thermosphere are very influential in the overall dynamics of the upper atmosphere because of their effects on the electric field (Chen JJ and Lei JH, 2019), which carries technological implications. They are closely tied to space weather phenomena, such as geomagnetic storms, solar flares, and coronal mass ejections. These disturbances can substantially alter the composition of the thermosphere (Cai XG et al., 2021) and the dynamics of the ionosphere (Ambili and Choudhary, 2022; Seba et al., 2022) through modulation of the ionospheric current system (Hamid et al., 2021). Throughout the years, attempts to measure TNWs have typically been done in one of two ways: ground-based instrumentation through incoherent scatter radars (ISRs), ionosondes, and Fabry–Perot interferometers (FPIs), or space-based data collection via satellite measurements. Additionally, empirical and first-principle models have historically been used to gain insight into the processes driving TNWs and governing upper atmospheric dynamics. In summary, the interplay between external drivers and the inherent dynamics of the Earth's upper atmosphere highlights the need for a multidisciplinary and holistic approach to unraveling the complexities of this intricate system.

In this review, we are interested in the equatorial region, which holds a certain geometrical significance because of its nearly horizontal magnetic field lines parallel to the surface of the Earth. This distinction is crucial for studying the dynamics and phenomena occurring in the upper atmosphere. Specifically, plasma particles in the upper atmosphere are influenced by the Earth's magnetic field, and studying their behavior along the magnetic equator allows scientists to observe and analyze the effects of magnetic forces on these particles. In particular, the climatology of winds over the magnetic equator exhibits unique phenomena primarily because of the geometry of the Earth's magnetic field, where the zonal component of the wind is perpendicular to the field and the meridional component aligns with the field (Sivla et al., 2020). Moreover, the magnetic equator is an important region for studying the interactions between the Earth's magnetic field and incoming solar radiation. Solar radiation interacts with the Earth's magnetic field differently at the dip equator compared with other latitudes. This unique interaction leads to the formation of phenomena such as the equatorial electrojet (EEJ) and equatorial ionization anomaly (EIA). These phenomena interact with the TNWs, leading to changes in circulation patterns, which have significant implications for communication systems, satellite operations, and our overall understanding of space weather.

This review article aims to tackle the challenges and gaps in understanding TNWs in the equatorial region by offering an overview of historical neutral wind measurements at low latitudes. Additionally, it delves into the current operational ground-based and space-based missions, which furnish valuable information on TNWs, along with their limitations. The article further explores the ionospheric and thermospheric phenomena specific to the equatorial region and their interactions with neutral winds. Overall, this review emphasizes TNWs and their influence by processes at subtropical latitudes, stressing the necessity for comprehensive measurements in the equatorial region. These efforts aim to enhance our understanding of their role in global atmospheric dynamics and improve weather forecasting capabilities.

2. Observation of Thermospheric Winds

2.1 Ground-based Instruments

One method of observing TNWs is through the use of ground-based instruments. This approach is often used to gather thermospheric and ionospheric data over a specific region, with a focus on temporal variations. Stationary instruments provide continuous data collection in one location throughout each day, making them useful for identifying long-term trends in TNWs. However, most observational data have been confined to the middle (Sivla and McCreadie, 2014; Harding et al., 2019; Navarro and Fejer, 2020) and upper (Lu G et al., 2016; Xu H et al., 2019; Oyama et al., 2023) latitudes. Only in the past couple of decades have more reliable *in situ* instruments, such as the FPI, been installed in equatorial locations. In this section, we examine the instruments that have historically been used for TNW measurements.

The earliest attempts at measuring TNWs date back to the 1960s and utilized radars, such as the ISRs proposed by Gordon (1958), to directly measure the properties of ionized plasma in the upper atmosphere. These radars use the incoherent scattering of radio waves off free electrons and ions to gather information about ions and electron density. From these measurements, TNW velocity in the region of study can be derived through various models (Kofman et al., 1986; Farmer et al., 1990; Davis et al., 1995). Specifically, the motions of the neutral atmosphere are extracted from

measurements of the motions of the ionospheric plasma along the line-of-sight of the radar, which results in the introduction of a Doppler shift in the measured scatter spectrum proportional to the drift velocity of the ions and electrons (Salah and Holt, 1974). The incoherent scatter return signal spectrum is dependent on multiple ionospheric parameters: electron density, ion and electron velocities and temperatures, and ion composition (Evans, 1969). Through the use of ISRs, some key understandings regarding TNWs and the complex system formed in the thermosphere–ionosphere coupling have been discovered. For instance, Williams (1989) identified the source region for large-scale atmospheric gravity waves affecting the thermosphere based on neutral density parameters derived from profiles of electron concentration or field-aligned plasma velocity as measured with an ISR. Currently, several ISRs across the globe are still actively being used to observe upper atmospheric dynamics, such as the recent Sanya ISR, because of their ability to measure ionospheric contents at varying heights. The locations of the ISRs, alongside a number of other important instruments, including ionosondes and FPIs in the equatorial region, are listed in Figure 1 and Table 1. However,

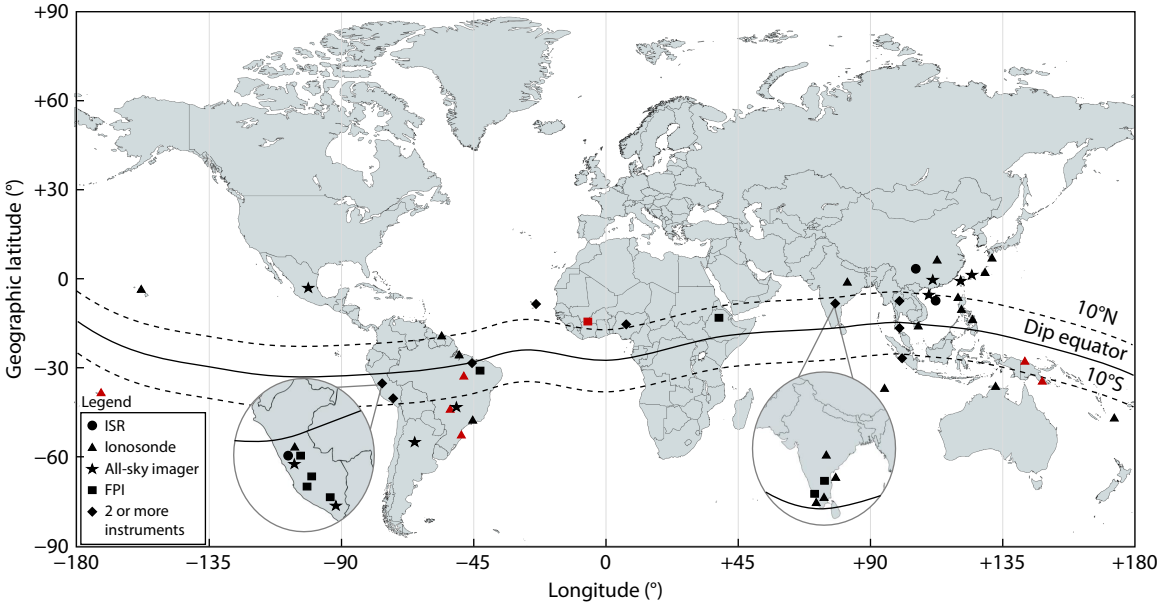

Figure 1. Past and current ground-based instruments for measuring TNWs in the low-latitude region (*less than* 25° of the dip equator). Instruments that are no longer in operation are marked in red.

Table 1. A nonexhaustive list of past and present ground-based stations for thermospheric wind measurement in the low-latitude and equatorial region.

Location	Dip latitude (°)*	Geographic longitude (°)	Instrument	Years in operation	References
Abuja	+10.6	+7.5	FPI	2016–present	Wu Q, 2016
			All-sky imager	2015–present	Okoh et al., 2017
Allahabad	+17.0	+81.8	Ionosonde	2015–present	Ramsingh et al., 2015
Arequipa	−7.1	−71.4	FPI	1983–present	Meriwether et al., 1986
			All-sky imager	1993–present	Colerico et al., 1996
Bac Lieu	+0.0	+105.7	Ionosonde	2004–present	Maruyama et al., 2007
Bahir Dar	+8.3	+37.4	FPI	2015–present	Tesema et al., 2017
Boa Vista	+11.9	−60.7	Digisonde	2002	Abdu et al., 2009
			All-sky imager	2013–present	Paulino et al., 2011
Cachimbo	−0.7	−54.8	Digisonde	2002	Abdu et al., 2009
Cachoeira Paulista	−14.4	−45.0	Digisonde	2002	Abdu et al., 2009
				1990–present	Fagundes et al., 1995
					Batista et al., 2000
			FPI	1988–present	Sahai et al., 1994
			All-sky imager	1987–1991	
Cajazeiras	+0.8	−38.6	FPI	2009–present	Makela et al., 2009
Campo Grande	−11.7	−54.6	Digisonde	2002	Abdu et al., 2009
			All-sky imager	2013–present	

Continued from Table 1

Location	Dip latitude (°)*	Geographic longitude (°)	Instrument	Years in operation	References
Cariri	−4.4	−35.0	All-sky imager FPI	1972–present 2009–present	Medeiros et al., 2004 Makela et al., 2009
Carmen Alto	−3.9	−69.4	FPI	1996–present	Martinis et al., 2001
Cebu	+9.9	+195.6	Ionosonde	~1998–present	Maruyama et al., 2002
Chiang Mai	+9.6	+98.9	Ionosonde FPI	2004–present 2010–present	Maruyama et al., 2007 Shiokawa et al., 2012
Chumphon	+1.6	+99.4	Ionosonde All-sky imager	2004–present 2020–present	Maruyama et al., 2007
Cocos Islands	−21.3	+96.9	Ionosonde	1961–present	Kalita et al., 2016
Darwin	−21.0	+130.8	Ionosonde	1982–present	Lynn et al., 2006
El Leoncito	−22.6	−69.4	All-sky imager	1999–present	Martinis et al., 2006
Fuke	+10.2	+109.1	All-sky imager	2013–present	Wu K et al., 2017
Guiping	+14.2	+110.7	All-sky imager	2013–present	Wu K et al., 2017
Hyderabad	+9.2	+78.5	Ionosonde	1963–present	Sreekumar and Sripathi, 2016
Ishigaki	+15.5	+124.2	All-sky imager	2014–present	Hosokawa et al., 2020
Jicamarca	−2.8	−76.9	ISR Digisonde All-sky imager	1961–present 1992–present 2014–present	Farley, 1991 Reinisch, 1993 Mendillo, 2015
Kavalur	+7.1	+78.5	FPI	1992–present	Sastri et al., 1994
Kodaikanal	+2.1	+77.5	Ionosonde	1955–present	Sastri et al., 1994
Korhogo	+13.0	−5.6	FPI	1993–1995	Vila et al., 1998
Kototabang	−9.4	+100.3	Ionosonde FPI	2004–present 2010–present	Maruyama et al., 2007 Shiokawa et al., 2012
Lulin	+14.5	+120.9	All-sky imager	2021–present	Liu JY et al., 2024
Manila	+5.6	+121.1	Digisonde	~1998–present	Maruyama et al., 2002
Maui	+21.5	−156.5	Ionosonde	1944–present	Bittencourt and Sahai, 1978
Merihill	−2.8	−76.9	FPI	2009–present	Gerrard and Meriwether, 2011
Nazca	−5.5	−74.5	FPI	2011–present	Navarro and Fejer, 2019
Niue	−23.1	+170.0	Ionosonde	2004–present	Wilkinson, 2005
Okinawa	+17.6	+127.8	Ionosonde	2001–present	Maruyama et al., 2004
Paramaribo	+14.7	−55.2	Ionosonde	1957–present	Bittencourt and Sahai, 1978
Port Moresby	−16.6	+147.1	Ionosonde	1961–2007	McNamara and Wilkinson, 2009
Qujing	+16.3	+103.8	ISR	2014–present	Ding ZH et al., 2018
Rarotonga	−20.4	−159.7	Ionosonde	1945–1980	Bittencourt and Sahai, 1978
Sanya	+9.0	+109.6	ISR	2020–present	Yue XA et al., 2022
São Luis	+5.7	−44.3	Digisonde	2002 1994–present	Abdu et al., 2009 De Paula et al., 2004
São Paulo	−15.2	−46.6	Ionosonde	1953–1965	Bittencourt and Sahai, 1978
Sriharikota	+5.4	+80.1	Ionosonde	1989–present	Sastri et al., 1994
Taoyuan	+16.0	+121.3	Ionosonde	1960–2000 2006–2016 2020–present	Ke KJ et al., 2022
Tirunelveli	+0.6	+77.8	Ionosonde	2006–present	Sreekumar and Sripathi, 2016
Trivandrum	+0.5	+77.0	Ionosonde FPI	1989–present 2017–present	Sastri et al., 1994 Hossain et al., 2023
Tucumán	−17.6	−65.0	All-sky imager	1997–1999	Martinis et al., 2003
Vanimo	−10.4	+141.3	Ionosonde	1964–2009	Lynn et al., 2006
Wuhan	+21.3	+114.4	Ionosonde	1946–present	Yue XN et al., 2018
Yamagawa	+24.6	+130.6	Ionosonde	1946–present	Maruyama et al., 2004

*Dip latitudes as calculated for the 2024.0 epoch.

this review does not go into detail on each of these data sources, their methodologies, or results.

Similar to ISRs are ionosondes, which are ground-based instruments that utilize radio waves to study the ionosphere. They emit radio waves at various frequencies and then detect the signals that are reflected from the ionosphere. This approach allows scientists to measure properties such as electron density, electron temperature, and ionospheric plasma drift. We owe a large number of early TNW observations to the ionosonde, which allowed for investigations to be carried out on the long-term variability of TNWs alongside ionospheric variations. For example, Haridas et al. (2016) made use of ionosonde data spanning two solar cycles to investigate the climatology of meridional winds and its variability with respect to solar activity over the Indian equatorial sector. When examining the thermosphere–ionosphere system (TIS), ionosondes are favored because of the widespread availability of ionosonde networks worldwide (Sreekumar and Sripathi, 2016). They also offer cost-effective data collection on the electron density profile (Hanbaba, 1995) while allowing neutral parameters to be derived from measurements of the height of the F_2 layer (Miller et al., 1986). However, this derivation of TNWs introduces uncertainties arising from several factors. First, the measured height of the F_2 layer peak (h_{max}) can have uncertainties because of limitations in the ionosonde itself. Additionally, the linear regression used to determine the proportionality constant (α) relating wind velocity and h_{max} might not perfectly fit the data points if substantial scatter is present. Another source of uncertainty is the ionospheric model used to determine α and the calculated height of the F_2 layer peak when wind velocity is zero (h_0), which neglects the effects of electric fields on the F layer. Thus, each of these factors can contribute to the overall uncertainty in determining the TNW velocity when using the height of the F_2 layer peak measured with the ionosonde.

In addition to radars, optical instruments have been used to directly measure the thermosphere through Doppler spectroscopy, via airglow imaging and interferometers. All-sky imagers, such as the high-latitude SCANning Doppler Imager (SCANDI), allow for measurements over a large field of view and thus are capable of observing thermospheric variabilities on spatial scales of several tens of kilometers (Aruliah et al., 2010). Presently, however, the most popular method of measuring TNWs is through the FPI, which holds an advantage over radars and ionosondes by providing very high resolution and direct measurements of important TNW parameters, namely, wind velocity and temperature, from emissions produced by neutral particles during dissociative recombination (Florescu-Mitchell and Mitchell, 2006). Operating on the principle of interference, the FPI utilizes multiple reflections within a resonant optical cavity to measure the Doppler shift of the incoming airglow emission (Makela et al., 2011). Through analysis of the interferogram pattern of fringes produced, the neutral wind velocities and temperatures can be derived with exceptional precision.

Each of the instruments presented in this section has its advantages and disadvantages based on the circumstances of the investigation being carried out, and there has yet to be an instrument capable of addressing all our knowledge gaps of TNWs arising from their spatiotemporal complexities. For specific investigations into TNWs, the FPI is arguably the best instrument because it provides direct and accurate measurements of neutral parameters with a reasonably satisfactory time resolution of up to 15 min (Shiokawa et al., 2012). One of the limitations of FPIs is that they are restricted to post-sunset observations only because of the overwhelming effect of atmospheric scattering during the daytime, which has been noted to introduce errors of up to 400 m/s (Harding et al., 2017a). Additionally, FPIs with fixed etalon spacings are also capable of measuring only one emission wavelength (typically the OI 630-nm airglow) at a time, leading to poor height resolution in the thermosphere. Thus, studies focusing on the TIS would benefit from utilizing instruments that are capable of measuring both neutral and ionospheric parameters, such as radars.

2.2 Space-based Instruments

Remote sensing observations conducted from high altitudes have been instrumental in advancing our understanding of TNWs. These satellite missions have provided us with data on the horizontal and vertical components of neutral winds, giving us valuable insights into the global distribution, altitudinal variations, and temporal dynamics of neutral winds in the upper atmosphere. The instruments onboard the satellites are highly crucial in determining the types of information that can be gathered on the upper atmosphere and the accuracy of data collected. The satellite observatories that have historically measured TNWs are summarized in Figure 2.

The first multiyear satellite mission capable of specifically measuring thermospheric neutral parameters over the equatorial region was the Atmosphere Explorer-E (AE-E), which was equipped with a spectrometer to measure the velocity distribution of molecular nitrogen, enabling the derivation of the temperature of the neutral gas (Spencer et al., 1973). Throughout its 3 years of operation, the AE-E orbited at different heights between 250 and 450 km, which allowed for the analysis of TNW changes with varying altitudes. Using measurements from the AE-E, Herrero et al. (1988) reported weaker poleward meridional winds in winter, with a maximum occurring in the early evening sector, whereas in the summer, winds were stronger and peaked closer to midnight. Following the success of the AE-E, the Dynamics Explorer 2 (DE-2) was launched in 1981, featuring the unique ability to measure the vector wind field of the neutral atmosphere, along with a comprehensive set of other thermospheric, ionospheric, and magnetospheric variables (Killeen and Roble, 1988). This measurement was achieved through the FPI (Hays et al., 1981) and the Wind and Temperature Spectrometer (WATS) onboard. The Upper Atmosphere Research Satellite (UARS) was another early spacecraft capable of measuring TNWs with its onboard Wind Imaging Interferometer (WINDII), providing us with wind measurements covering the entirety of Solar Cycle 22 (Reber et al., 1993). The data collected from these early satellite observatories proved valuable in refining existing empirical and physics-based models. Such is the case with the Mass Spectrometer–Incoherent Scatter (MSIS)-86 model by Hedin (1987), which was updated with neutral temperature, density, and composition data from the DE-2 mission.

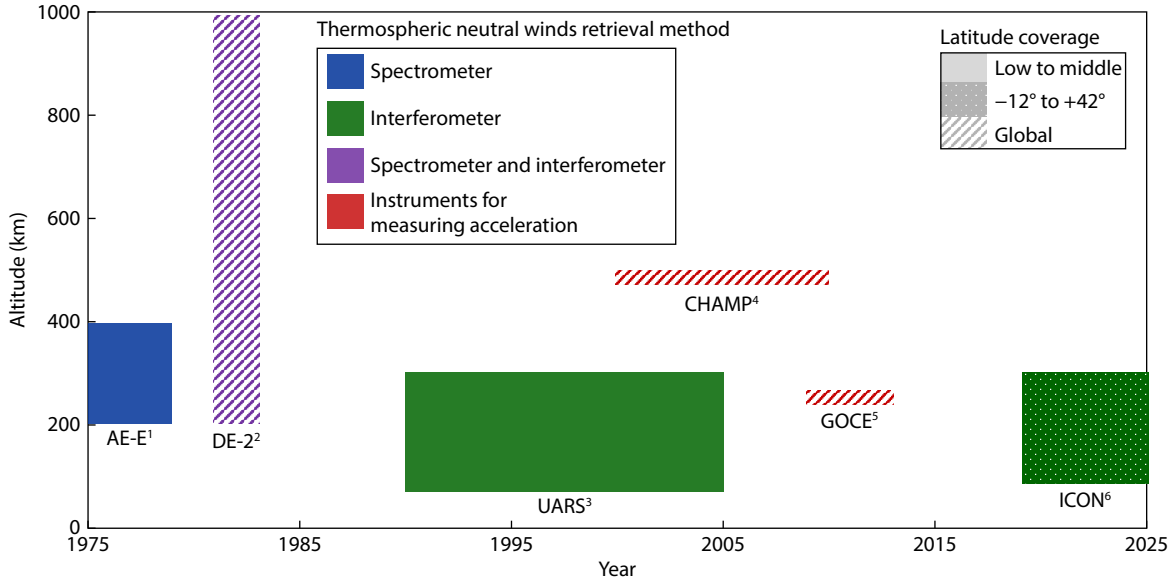

Figure 2. Past and current satellite observatories capable of measuring low-latitude TNWs. From [1]Pelz et al., 1973; [2]Hoffman and Schmerling, 1982; [3]Reber et al., 1993; [4]Reigber et al., 2002; [5]Drinkwater et al., 2007; and [6]Immel et al., 2018.

Satellites with global coverage have also been used to study TNWs over the low-latitude region, namely the German CHAllenging Minisatellite Payload (CHAMP), and the Gravity Field and Steady-State Ocean Circulation Explorer (GOCE). Zonal wind measurements obtained from accelerometers on CHAMP were used in multiple TNW studies. For instance, Sutton et al. (2005) illustrated the spatial–temporal dependence of the thermospheric response to the severe solar storms occurring from October 29 to November 1, 2003. In contrast, GOCE was a mission mainly aimed toward measuring the Earth's static gravity field at a high spatial resolution and accuracy (Drinkwater et al., 2007); however, measurements made with the onboard gradiometer and ion thruster could be used to determine air density and crosswind speed in the Earth's thermosphere (Doornbos et al., 2013). With the help of increasingly accurate GOCE measurements of TNWs, our understanding of other upper atmospheric phenomena has been improved. For instance, by conducting simultaneous observations of TNW velocities obtained from the GOCE over Southeast Asia from 2010 to 2013 and measuring the EEJ strength by using ground-based magnetometers, Abadi et al. (2021) proposed that eastward winds and the EEJ are likely to independently influence the pre-reversal enhancement (PRE) of the eastward electric field in the evening equatorial ionosphere, with their effects balancing each other.

At present, only one active satellite observatory is capable of measuring both ionospheric and neutral thermospheric parameters over the equatorial region. This is the Ionospheric Connection Explorer (ICON) launched in 2018 to join the National Aeronautics and Space Administration's heliophysics satellite constellation. Its primary scientific objective is to identify the sources of strong ionospheric variability. In the low-latitude equatorial region, where the ionosphere is shielded from magnetospheric and solar wind influences, it is suggested that the main sources of this variability are neutral wind circulation and ionospheric conductance (Immel et al., 2018). Therefore, to study this thermosphere–ionosphere coupling, the ICON satellite measures neutral winds in the range of the dynamo region (~100–160 km) via remote sensing limb measurements, along with local ion drift measurements for a limited time period (Harding et al., 2017b). The ICON is equipped with the Michelson Interferometer for Global High-Resolution Thermospheric Imaging (MIGHTI), which utilizes two perpendicular fields of view pointed at the Earth's limb to measure the Doppler shift of the atomic oxygen red and green lines at wavelengths of 630.0 nm and 557.7 nm, respectively (Englert et al., 2017).

In addition to long-term satellite missions, *in situ* measurements have frequently been used to investigate upper atmospheric dynamics for short windows of time, which has provided us with knowledge on (1) mesospheric and lower thermospheric winds, and (2) thermospheric–ionospheric responses to space weather events, such as geomagnetic storms. These systematic observations have been conducted via sounding rockets (Pfaff et al., 2020), which can provide good height resolution and broad altitude coverage (Larsen, 2002), as well as balloon-borne optical instruments (Wu Q et al., 2012), which allow for daytime measurements of TNWs. However, these observations have been mostly focused on the middle to high latitudes only (Heppner and Miller, 1982; Deng Y et al., 2017), with very few missions carried out over near-equatorial regions (Anandarao and Raghavarao, 1979; Larsen and Odom, 1997).

2.3 Modeling Approach

Various modeling techniques have been used to study and understand the dynamics of the thermosphere, including the behavior of neutral winds. The integration of these diverse modeling techniques has substantially enhanced our ability to comprehend the complex dynamics of TNWs, paving the way for more accurate predictions and a deeper understanding of Earth's upper atmosphere. These models have not only improved our understanding of the thermosphere and its interactions with the space environment, but also have practical applications in various fields (Ren ZP

et al., 2009). Two approaches can be used to model the complex upper atmospheric system: (1) through empirical models that integrate observational data collected throughout the years, and (2) through first-principle models that predict neutral dynamics based on physical processes, by taking into account factors such as solar activity and geomagnetic conditions.

The most well-developed empirical model is the Horizontal Wind Model (HWM), which has been updated several times since its conception in the 1990s, the latest version being the HWM14. The HWM integrates various data from quiet-time TNW observations; however, a large portion of the data integrated into the current HWM14 are sourced from mid- to high-latitude observations, which naturally means that the model does not perform very well when simulating low-latitude or subtropical winds (Okoh et al., 2021; Rabiu et al., 2021). The model also does not reproduce solar radiation flux variations very accurately (Haridas et al., 2016), which is why the Disturbance Wind Model (DWM) was later developed to simulate wind dynamics more accurately during geomagnetically disturbed conditions. Additionally, these models are subject to data sparseness at certain altitudes and time ranges (Drob et al., 2008, 2015). At present, because of the lack of observational data collection in the equatorial region, newly developed empirical models, such as the Magnetic mEridional NeuTrAl Thermospheric (MENTAT) model (Dandenault, 2018) and the High-Latitude Thermospheric Wind Model (HL-TWiM; Dhadly et al., 2019), mostly incorporate data from middle to high latitudes; hence, they may not perform well at modeling the equatorial region. In time, as the global TNW data collection network expands, these latitudinal gaps in existing empirical models can eventually be resolved. Additionally, there also exist empirical models that simulate other parameters of the thermosphere, including temperature and density. Such is the case with the MSIS-86 model (Hedin, 1987) and its numerous iterations. Although these models do not provide direct simulation of TNWs, they may provide supplementary information on thermospheric conditions, which helps in explaining any behavioral changes in TNWs. For instance, Murty and Kim (1988) utilized the MSIS-83 and MSIS-86 models to identify an increase in thermospheric temperature during disturbed storm-time conditions, which helped explain the enhanced equatorward meridional winds observed with the FPI. The MSIS models have also been used in combination with the HWM to provide comparisons with observational data, as can be seen in the work by Wu Q et al. (1994). Hence, it is evident that oftentimes models that only simulate TNWs may not sufficiently explain wind circulation patterns and may require additional modeling of upper atmospheric conditions to provide a more comprehensive understanding of TNW behavior. This shortcoming highlights a need for improved thermospheric models that incorporate multiple parameters of the thermosphere.

On the other hand, first-principle models have opened new possibilities for studying and predicting the behavior of TNWs in different regions and under various environmental conditions (Harding et al., 2019). One prominent modeling technique used in TNW studies is the Thermosphere–Ionosphere Electrodynamics General Circulation Model (TIEGCM), which is a three-dimensional (3-D), nonlinear representation of the TIS that includes a self-consistent solution of the low-latitude dynamo electric field (Jiang GY et al., 2018). The TIEGCM improves on its previous versions by incorporating mid- and low-latitude electrodynamics. Thus, it produces more accurate models during storm-time periods because of its emphasis on the coupling of the TIS that occurs during strong geomagnetic disturbances. Another model similar to the TIEGCM that is often used is the Global Ionosphere–Thermosphere Model (GITM), which is a comprehensive numerical model that considers solar activity variations when simulating the global ionosphere and thermosphere system, including neutral winds. The GITM solves the Navier–Stokes equations for the thermosphere, broken into vertical and horizontal directions and considering ion drag, Coriolis, pressure gradients, and geometric terms (Ridley et al., 2006). Thus, by incorporating key physical processes, such as solar radiation, chemical reactions, and interactions between different atmospheric constituents, the GITM provides valuable insights into the behavior of TNWs under varying conditions. Nevertheless, Harding et al. (2019) reported that correlations with data collected by using the FPI are nearly zero at low latitudes. This finding suggests that substantial work is still required with the GITM before it can reliably predict daily variations in upper atmospheric weather over the geomagnetic equator.

Generally, the TIEGCM is regarded as the most capable physics-based model for simulating the low-latitude TIS, particularly regarding electron densities and ionospheric temperatures. Despite this capability, the model is still lacking in some ways, as seen in the study by Fesen et al. (2002), which identified discrepancies in multiple parameters, including horizontal neutral winds, when compared with observational data from equatorial stations in Peru. Additionally, Marsal et al. (2012) noted some limitations in capturing shorter term variations and height resolution with the TIEGCM. New models are actively being developed to better simulate TNW patterns and upper atmospheric dynamics in the equatorial region. For example, one of the more recent models that has been produced is the Global Coupled Ionosphere–Thermosphere-Electrodynamics Model, Institute of Geology and Geophysics, Chinese Academy of Sciences, (GCITEM-IGGCAS). One of the promising features of this model can be seen in its ability to simulate the EIA and midnight temperature maximum (MTM) at low latitudes (Ren ZP et al., 2009), a capability that the TIEGCM has not been able to replicate (Colerico et al., 2006). However, additional comparisons with observational data are necessary to verify its performance in equatorial TNW modeling. Another promising model is the Whole Atmosphere Community Climate Model with thermosphere and ionosphere extension (WACCM-X), which provides a comprehensive, self-consistent description of the entire atmosphere–ionosphere system, from the surface to an altitude of 500–700 km (Liu HL et al., 2010, 2018). This model is unique compared with the previously mentioned models, which had more limited representations of upper atmospheric processes. The WACCM-X has been useful for modeling low-latitude middle-atmosphere winds, which are lacking in terms of empirical observations because of instrument limitations (Dhadly et al., 2023). For instance, Venkat Ratnam et al. (2019) identified long-term wind trends in the lower thermosphere over the near-equatorial Indian sector, which they suggested were influenced by changes in concentrations of greenhouse gases, as simulated

with the WACCM-X. Besides providing insights into wind circulation at varying altitudes, the WACCM-X allows for investigations into lower atmospheric influences on thermospheric circulation by incorporating climate and weather processes into the model. For example, Liu HL et al. (2023) simulated traveling ionospheric disturbances (TIDs) resulting from a powerful volcanic eruption in 2022, which was observed to cause large wind perturbations in the thermosphere. Comprehensive, whole-atmosphere numerical models, such as the WACCM-X, which bridge meteorological processes with upper atmospheric dynamics, may prove to be quite crucial in future efforts to improve our current understanding of the global atmospheric system. However, observational data are still necessary to accurately constrain these whole-atmosphere models, as discussed by Sassi et al. (2021), who noted that the absence of middle-atmosphere data leads to substantially larger amplitudes of solar nonmigrating tides in WACCM-X simulations.

In more recent years, machine learning (ML) techniques have been emerging in the field of space weather, as discussed in the review by Camporeale (2019). Specifically, ML is becoming more prevalent in atmospheric studies for forecasting and nowcasting applications, mainly because of the turbulent nature of the upper atmosphere. Machine learning methods are known to be ideal for problems in which the relationship between input variables and the desired output is unknown or the physical model is computationally expensive because they effectively learn from data to handle complex, nonlinear systems. The TIS can be described as one such system, thus making it well-suited for ML techniques such as neural networks and generative modeling. Another reason that upper atmospheric research is suitable for ML applications is the increasing number of high-resolution datasets accumulated over the years through the various remote and *in situ* space missions discussed previously. However, most existing research using ML and deep learning techniques in thermospheric studies has focused on other parameters of the TIS, such as total electron content (TEC) predictions (Cai YH et al., 2019; Zewdie et al., 2021), long-term trends in thermospheric neutral density (Weng LB et al., 2020), and short-term forecasting of their responses to geomagnetic storms (Wang YR and Bai XL, 2022), with less emphasis on TNWs. This focus is likely due to the limited availability of large datasets of TNW observations, as discussed earlier in this section. Recent studies have demonstrated some promising effectiveness of ML techniques in developing forecasting models for near-space wind fields with errors of <5 m/s (Sun XX et al., 2024), which suggests that ML methods may be useful for forecasting upper atmospheric winds as well. As TNW datasets expand in coming years, ML is expected to play a more important role in TNW forecasting and consequently improve our understanding of the broader TIS through advanced techniques, such as feature extraction, which allow the analysis of multiple other variables of the system, such as temperature and density.

2.4 Comparisons Between Instruments and Approaches

Thermospheric neutral winds can be more conveniently understood as a large-scale 3-D fluid circulating globally; thus, it is spatially complex in terms of latitudinal, longitudinal, and altitudinal variations. One important aspect to consider is the latitudinal variation of these winds, which is influenced by the Earth's curvature and the distribution of solar heating. At higher latitudes, the neutral winds are influenced by the interaction of the Earth's magnetic field and the solar wind, leading to unique patterns of wind circulation. Simultaneously, pressure gradients resulting from thermal expansion push winds away from the geographic equator, which receives most of the solar heating on a day-to-day basis. Moreover, TNWs vary with longitude because of the difference in geomagnetic field configuration in the two hemispheres with different dip angles, inclinations, and magnetic field strengths (Wang WB et al., 2021). This difference leads to substantial variations in the ionosphere at different longitudes because the ionosphere layer is strongly regulated by the electromagnetic field. Therefore, ion drag forcing on TNWs is more pronounced at locations with higher ionospheric electron densities, such as places with weak PRE, as discussed by Yizengaw et al. (2014). Furthermore, altitudinal variations in TNWs are equally crucial because they are affected by the changing thermal structure of the upper atmosphere, the presence of gravity waves, and the influence of tides propagating from the lower atmosphere. Each of these variations leads to intricate vertical wind patterns that play a pivotal role in shaping the dynamics of the TIS.

It is crucial to emphasize that obtaining a comprehensive measurement of equatorial TNWs solely by using any single instrument would be challenging because each approach is affected by a drawback in one way or another. For example, despite their usefulness in identifying low-latitude and global wind circulation patterns at varying altitudes, space-based observatories are affected by the temporal dependence of TNWs owing to their inability to collect data continuously in any one location as these satellites orbit the Earth. Conversely, the spatial coverage of ground-based measurements may be limited, resulting in geographic sparseness of wind measurements even after combining data from multiple missions. Ideally, a combination of both ground-based and space-based observations supplied with simulations would provide an in-depth understanding of the processes influencing the climatology of equatorial TNWs and their impacts on upper atmospheric dynamics. Therefore, to enhance our comprehension of upper atmosphere dynamics over the equatorial region, it is vital to reduce data gaps by establishing a comprehensive data network, such as the Southeast Asia Low-Latitude Ionospheric Network (SEALION; Maruyama et al., 2007), as shown in Figure 3. Such data networks would cover various locations along the magnetic equator and be capable of measuring parameters of the chemical species of the TIS at varying altitudes. To reach this goal, governments, research institutions, and space agencies could jointly fund and maintain instruments across different geographic regions, allowing for shared use and operational costs, which would require international collaborative efforts. Establishing a global network of instruments for measuring TIS parameters would be a highly collaborative process with great potential, although some challenges would also need to be overcome. The major issues that should be considered are how instruments can be calibrated and synchronized to work together and how they can be installed. Moreover, the problems can be addressed through overcoming geographical and political constraints, fast data transfers, and data latency reduction, as well as data robustness in remote regions. On the other hand, mainte-

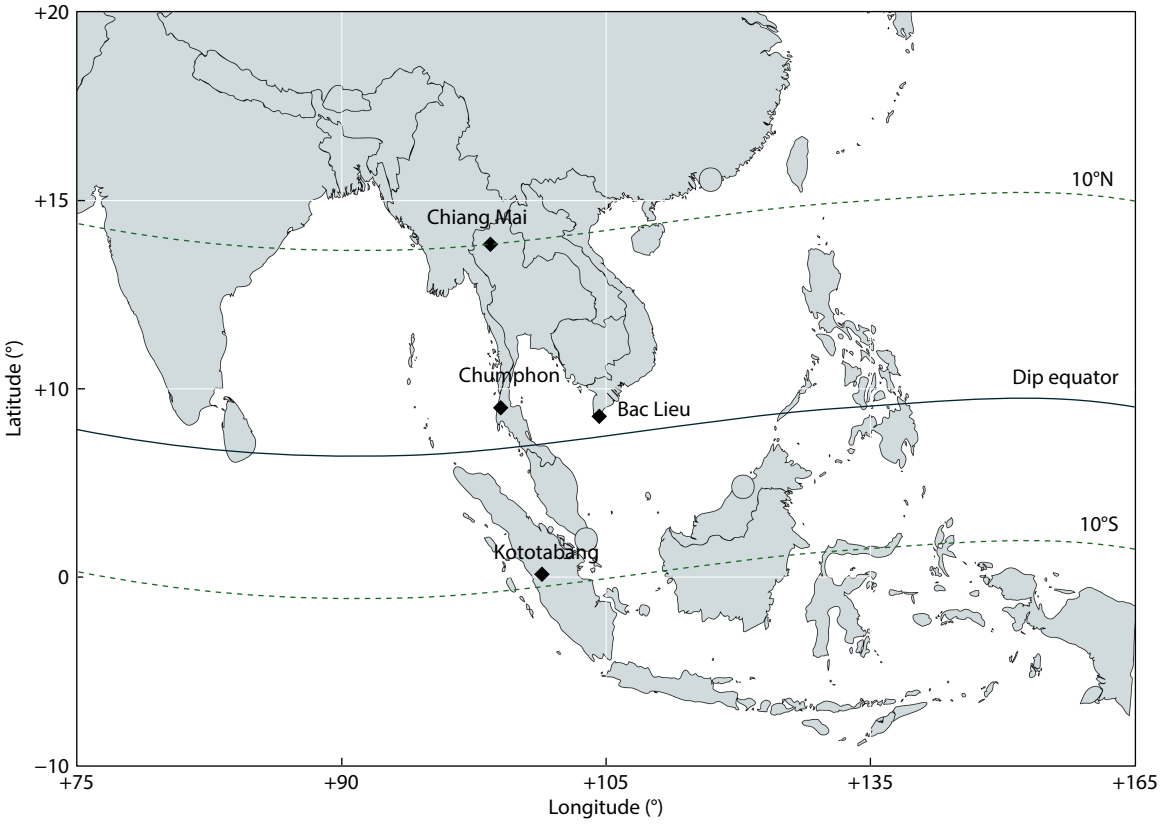

Figure 3. The location of each instrument in SEALION.

nance problems, such as adverse weather conditions and the processing of large data sets, require a resilient infrastructure and high-performance computing resources. In addition, concerns about data security, privacy, and standardization must be taken into account to make the global TNW data network a reality. However, overcoming these challenges and building strategic partnerships would be an important step forward for the better understanding of TNWs, and subsequently, the TIS.

In addition to reducing data gaps, improving data acquisition tools is another method that could be used to obtain a comprehensive understanding of the TIS and TNWs. To this end, several new instruments have been proposed, such as the Doppler Wind and Temperature Sounder (DWTS) suggested by McHugh et al. (2014). The DWTS is designed to be operated on a spacecraft and utilizes Doppler-modulated gas correlation and spectroscopy to measure the Doppler shift of atmospheric emission lines. This capability allows it to determine wind speeds and air temperatures at multiple altitudes, operating days and nights to offer high temporal resolution. Another promising space-based instrument is the Terahertz Limb Sounder (TLS), which is designed to measure atmospheric properties such as wind, oxygen density, and temperature by observing emissions at terahertz frequencies (Wu DL et al., 2016). The mechanism involves using terahertz receivers to detect emissions from molecular oxygen and atomic oxygen specifically in the Earth's lower thermosphere. These instruments may be used to gain insight into equatorial TIS dynamics if deployed on satellite missions orbiting at low latitudes. As for ground-based instruments, few novel methods have been proposed in favor of optimizing existing technologies. An example that enhances current interferometers and has applications both in space and on the ground is Doppler Asymmetric Spatial Heterodyne (DASH) spectroscopy (Englert et al., 2007). Doppler Asymmetric Spatial Heterodyne spectroscopy operates in a manner similar to the Michelson interferometer used in WINDII. It holds an advantage over typical FPIs and interferometers by being compact and allowing simultaneous observations of multiple spectral lines, which means that it can offer good height resolutions (Marr et al., 2012). Comparisons with ground-based FPIs in mid-latitude regions show generally good agreement, with occasional disagreements larger than the combined uncertainties attributed to cloud interference and differences in observation geometry (Englert et al., 2012). Although novel ground-based techniques and instruments have been emerging in recent times (e.g., DopplerWind lidars; Liu ZL et al., 2019), at present these instruments have yet to be deployed along the magnetic equator. Instead, making improvements to current instrumentation techniques (e.g., Chen G et al., 2009; Gerrard and Meriwether, 2011) seems to be the focus in ground-based equatorial TNW research.

3. Climatology Studies of Neutral Winds

3.1 Characterizing Winds

Variations in TNWs can be complex because of the myriad factors influencing them. Therefore, a large part of thermospheric studies is dedicated to characterizing the behavior of TNWs and identifying the mechanisms influencing any deviation from their typical behavior. During periods of high solar and geomagnetic activity, the thermosphere and ionosphere form a complex and intricate

coupled system whereby the neutral constituents of the thermosphere interact with the ionized plasma of the ionosphere. In the low-latitude equatorial region, the effect of this coupling becomes more pronounced as the zonal component of the TNW generates electric fields by transporting ions along the magnetic field lines through a dynamo process (Heelis and Maute, 2020). Few long-term studies have been undertaken on TNW variability with solar activity, which fluctuates over an 11-year cycle. Therefore, its effects on TNWs are still under investigation. Additionally, investigations looking into the comparisons of TNW behavior across solar cycles are lacking. In their project encompassing two solar cycles, Haridas et al. (2016) discovered that equatorward meridional winds during low solar activity (indicated by the $F_{10.7}$ cm solar radio flux index) were higher by 30 m/s compared with high solar activity. This increase could potentially be due to reduced ion drag forcing. Similarly, by utilizing zonal wind data from the CHAMP satellite to statistically determine TNW variations with solar flux, Zhang XF et al. (2017) found that eastward zonal winds are reduced during periods with high solar flux levels.

The interaction between the solar wind and the Earth's magnetosphere can result in the formation of geomagnetic storms, which subsequently affect the behavior of neutral winds in the thermosphere. Strong geomagnetic disturbances have been observed to coincide with reduced wind velocity amplitudes caused by alterations in solar heating and increased Joule heating. Additionally, these disturbances can stem from collisions between neutral particles and convecting ions in the thermosphere (Fejer et al., 2017). Westward winds during geomagnetically disturbed conditions may result in increased energy and momentum deposition into the ionosphere at high latitudes (e.g., Blanc and Richmond, 1980; Fuller-Rowell et al., 1997), which drives the disturbance wind dynamo. Additionally, thermospheric neutral density has been noted to undergo enhancements of up to 200%–300% (Sutton et al., 2005), which spread to equatorial latitudes because of equatorward winds. The effects on TNWs and the equatorial electric fields may persist into the post-storm recovery phase, as observed by Polekh et al. (2017), where westward and polarized jets caused thermospheric Joule heating, which increased TNW velocity and generated disturbed dynamo electric fields over the low-latitude region during the recovery phase of the March 17–19, 2015, geomagnetic storm. In summary, all phases of a geomagnetic storm can cause disturbances in the TIS, resulting in substantial alterations in the circulation patterns and temperatures of TNWs. A comparison of quiet-time and storm-time wind patterns, as modeled by the HWM and its disturbance counterpart the DWM during midnight Coordinated Universal Time (UTC), are shown in Figure 4, where the reduction in wind velocity during disturbed conditions is apparent. It can also be seen that equatorial winds are generally lower velocity than those at upper latitudes during both geomagnetic conditions.

As emphasized previously, TNWs are temporally and spatially complex structures that undergo modulation throughout each day and exhibit variations between different months and seasons. One key aspect of the seasonal variability in the thermosphere is the influence of solar radiation. The varying intensity and angle of incidence of solar radiation throughout the year result in substantial changes in the upper atmosphere. As a result, this influences the TNWs, which lead to distinct seasonal patterns. During the equinoxes, when the Sun is directly over the equator, the TNWs exhibit a relatively symmetrical and balanced pattern, with winds flowing from the east to the west (Tsuda et al., 2016). During the summer months (May, June, July), the intensity of solar radiation increases, resulting in a reoccurring MTM, which reduces zonal wind velocities, as shown by Makela et al. (2013) between the years 2009 and 2012. The authors also observed that the meridional winds showed trans-equatorial flow from the summer to winter hemisphere, which is consistent with the findings of Hari and Krishna Murthy (1995). The winter solstice months (November, December, January) respond to stronger eastward winds, as shown by Liu HX et al. (2016) based on GOCE observations in 2010–2013, which agreed with 2017 trends in the African longitudinal sector, as demonstrated by Sivla et al. (2020).

Finally, TNWs also show variability with local time because of daily fluctuations in the thermal responses to solar activity. Previous studies have shown that during geomagnetically quiet times in the low-latitude equatorial region, zonal winds are mostly eastward and that they peak during pre-midnight hours, a few hours after sunset (Tesema et al., 2017; Rabiu et al., 2021; Sarudin et al., 2022). Differences may be seen in terms of wind velocity amplitude because of varying ion drag influences in different longitudinal sectors (Hossain et al., 2023). In contrast, meridional winds are slightly more poleward during pre-midnight hours and peak near midnight, with a distinct reversal in direction caused by the pressure bulge associated with the MTM, as first noted by Harper (1973) and again in subsequent observations at other equatorial latitudes (Spencer et al., 1979; Niranjan et al., 2006; Maruyama et al., 2008). Figure 5 provides an overview of quiet-time wind patterns and their relation to magnetic declination and electric content at midnight UTC. The winds are modeled by HWM and DWM, whereas the magnetic declination for the epoch of 2020 is obtained from the International Geomagnetic Reference Field (IGRF) model (Alken et al., 2021) provided by the International Association of Geomagnetism and Aeronomy (IAGA). The Coupled Thermosphere Ionosphere Plasmasphere Electrodynamics (CTIPe) model (Millward et al., 2001) was used to simulate TEC. It is evident that TNW circulation is highly dependent on the geomagnetic field and global plasma motions.

3.2 Space Weather in the Equatorial Region

Thermospheric neutral winds play a crucial role in the development of the TIS, particularly in relation to the dynamics of ionospheric weather. The low-latitude region is particularly interesting because it is characterized by several unique space weather phenomena. The mechanism responsible for most features of equatorial anomalies results from electric fields produced by zonal winds driving E region ionization across the magnetic field lines, which map up into the F region to produce vertical drifts of ionization (Titheridge, 1995). In the following paragraphs, we elaborate on these anomalous phenomena and explore their interactions with the TNWs. In addition, a summary of these phenomena, alongside their measurement methods and spatial distributions, is provided in Table 2.

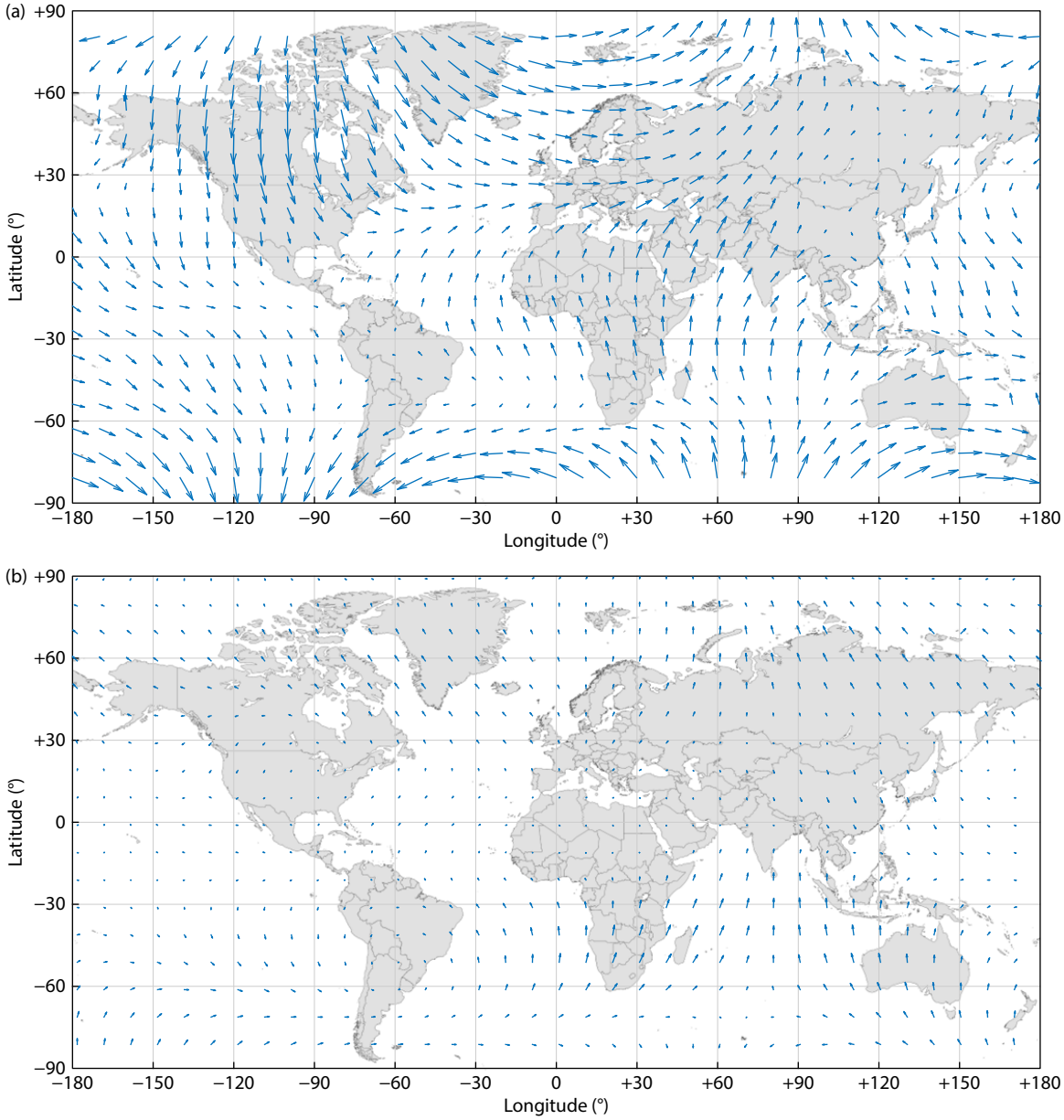

Figure 4. Thermospheric neutral winds at an altitude of 250 km during quiet and disturbed conditions at midnight UTC, modeled with (a) HWM14, and (b) DWM07. Wind velocity is indicated by the length of the vectors, where short-tailed arrows are lower velocity.

One of the most notable phenomena occurring in the equatorial region is the EEJ, which is an enhanced east–west overhead current restricted to within ±2° of the magnetic dip equator, exerting major influences on ionospheric conditions in the region, with little to no influence on the ionosphere outside this narrow strip (Bello et al., 2021). It is driven by the presence of boundaries inhibiting the flow of Hall current, resulting in a strong vertical polarization field that opposes the downward current flow, leading to the intense eastward Hall current known as the EEJ (Hamid et al., 2014). The existence of the EEJ is explained by the enhanced effective conductivity near the magnetic equator caused by inhibited vertical current flow (Forbes, 1981). Thermospheric neutral winds play a crucial role in shaping the height and latitude structures of the electrojet because they influence the dynamics of the EEJ region by pushing ions along magnetic field lines, causing northward or southward drifts while generating currents perpendicular to the magnetic field lines, as described in Figs. 9a, 9b, and 11 in the study by Reddy and Devasia (1981). Additionally, through the use of numerical simulations, Yamazaki et al. (2014) observed that the day-to-day fluctuations (up to ±25%) of the EEJ during calm periods are primarily influenced by zonal winds at altitudes of approximately 100–120 km near the magnetic equator. This observation was then confirmed in a later study utilizing Swarm magnetometer observations of EEJ intensity and wind velocities measured at different altitudes via MIGHTI, which showed that the EEJ correlated both positively (R = 0.58) and negatively (R = −0.54) with the equatorial zonal wind at heights of 110 km and 140 km, respectively. This potentially resulted in the reversal of the EEJ from its typical eastward direction to a westward current (Yamazaki et al., 2021). The westward current is also known as the counter electrojet (CEJ), which has been observed to correspond to a strong eastward zonal wind, as seen during the

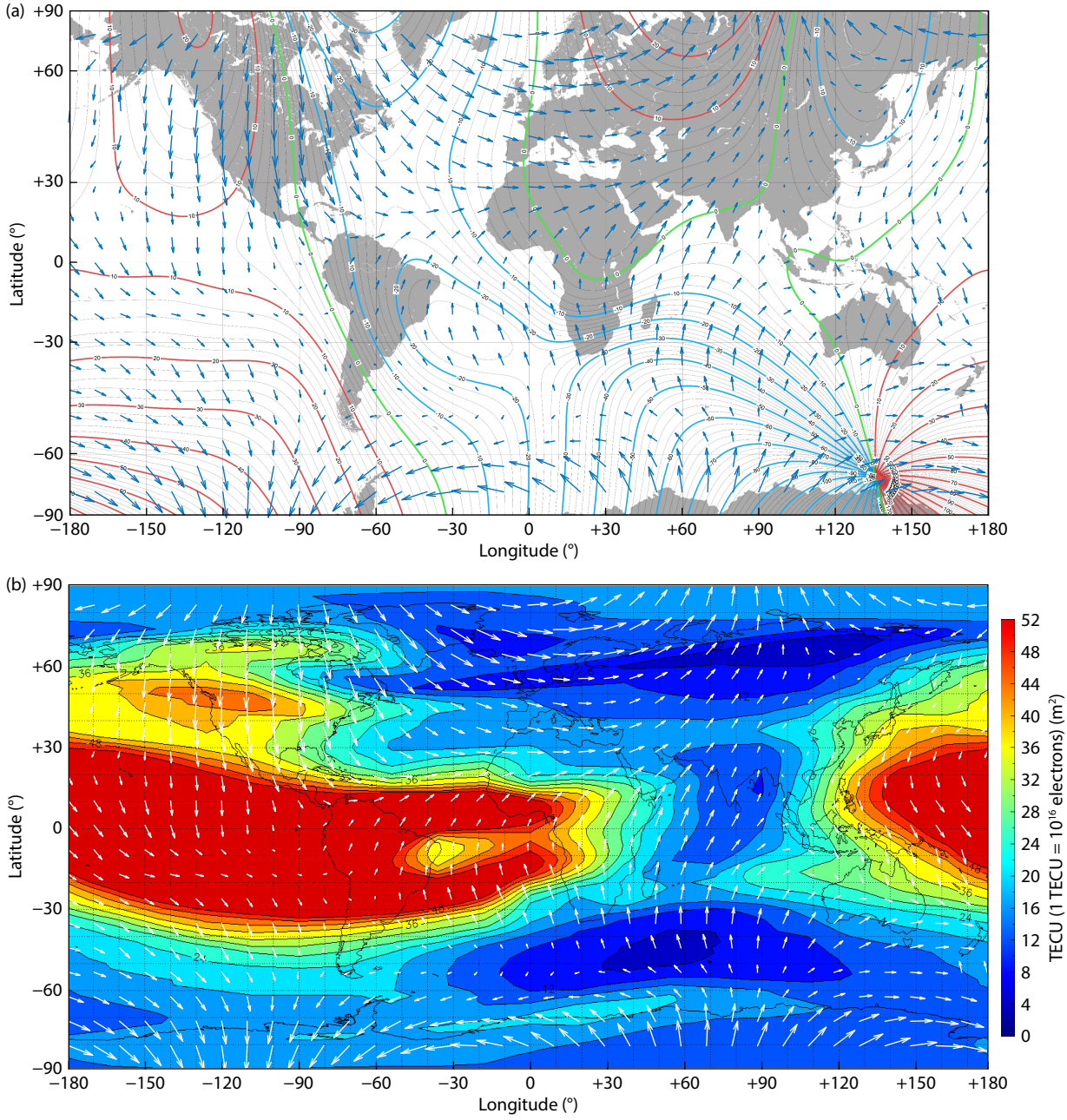

Figure 5. Quiet-time TNW patterns at an altitude of 250 km during midnight UTC as modeled by HWM14, overlaid with (a) the magnetic declination for epoch 2020 obtained from the IGRF model, where the red contour lines indicate positive degrees (east) and the blue contour lines indicate negative degrees (west), and (b) TEC unit (TECU) values simulated with the CTIPe.

Tonga volcanic eruptions that produced large-scale atmospheric disturbances leading to zonal wind reversal (Le G et al., 2022). Additionally, a study by Rosli et al. (2022) demonstrated that the CEJ could occur simultaneously at locations within 30° apart in longitude; however, an extensive simultaneous investigation has yet to be undertaken on the characteristics of TNWs and the CEJ in different longitudinal sectors to identify their influence on each other. Overall, the EEJ is strongly modulated by zonal winds, which are influenced by atmospheric forcing and solar activity, among other factors.

The EIA is another distinctive ionospheric phenomenon driven by the eastward electric field associated with the EEJ. It generates a pair of electron density crests at approximately ±15° latitude on both sides of the magnetic equator, a pattern that varies with solar activity. This anomaly results in a beltlike structure that flows eastward along the dip equator in the E region ionosphere (Balan et al., 2018). It also provides a region in the upper atmosphere where the neutral gas is heated by plasma–neutral collision (Qian LY et al., 2016). The meridional winds at low latitudes play a decisive role in the asymmetry of EIAs in the low-latitude ionosphere, as demonstrated by Khadka et al. (2018) through an investigation into the day-to-day variability of the EIA with simultaneous measurements of meridional winds. Meridional winds transport plasma up the field lines, thereby affecting the EIA configuration

Table 2. Space weather phenomena occurring in the equatorial region.

Phenomenon	Brief summary	Location	Detection	References
Equatorial electrojet (EEJ)	A narrow belt of strong eastward ionospheric current caused by electrodynamic coupling with the neutral atmosphere.	±2° of the dip equator at an altitude of 100–120 km	Magnetometer	Forbes, 1981
Equatorial ionization anomaly (EIA)	A belt of eastward currents with low electron density troughs formed on either side of the dip equator caused by plasma diffusion along geomagnetic lines, and upward $E \times B$ drift.	±15° of the dip equator	TEC from radars, ionosonde, and GPS	Balan et al., 2018
Equatorial temperature and wind anomaly (ETWA)	Anomalous latitudinal variations in zonal winds and temperature at low latitudes, with maximum and minimum differences exceeding 100 K and 100 m/s, respectively, caused by ion drag and possibly exothermic chemical reactions.	Zonal wind maximum at the dip equator with minima at the EIA crests; temperature maxima at EIA troughs and minima at the EIA trough	Interferometer, spectrometer	Raghavarao and Suhasini, 2002
Equatorial plasma bubbles (EPBs)	Geomagnetic field-aligned depletions of ionospheric plasma density caused by post-sunset recombination.	Bottomside F layer within ±15° of the dip equator	TEC from radars, ionosonde, and GPS	Rishbeth, 1971
Geomagnetic storm	Strong disturbance in the geomagnetic field caused by solar activity.	Upper atmosphere	Magnetometer	Burns et al., 1995
Midnight temperature maximum (MTM)	Large-scale neutral temperature anomaly accompanied by an increase in pressure and a poleward reversal in meridional winds.	Poleward propagation, with maxima at ±15° of the dip equator	Interferometer	Spencer et al., 1979
Traveling atmospheric disturbance (TAD)	Waves of perturbation in thermospheric density caused by Joule heating propagating toward low latitudes.	From high latitudes toward the equator	Satellite drag, accelerometer, spectrometer, interferometer	Hines, 1960
Traveling ionospheric disturbance (TID)	Waves of perturbation in density, velocity, and composition of ionospheric plasma, caused by geomagnetic disturbances and TADs.	From high latitudes toward the equator	TEC from radars, ionosonde, and GPS	Balthazor and Moffett, 1997

parameters, such as strength, shape, amplitude, and latitudinal width. Additionally, the EIA affects the zonal neutral winds, as noted by Martinis et al. (2001), where FPI observations of wind speeds at Carmen Alto, Peru, showed a ~20%–25% reduction compared with wind velocities at Arequipa, Peru, which is located closer to the magnetic equator. This difference was attributed to increased ion drag resulting from the higher electron density caused by Carmen Alto's proximity to the EIA crest. Hence, it is evident that the EIA and TNWs mutually influence each other in various ways; further real-time investigations into wind circulation patterns alongside EIA responses to magnetosphere-induced disturbances will be instrumental in improving our understanding of the intricacies involved in this relationship.

Furthermore, the equatorial temperature and wind anomaly (ETWA), sometimes generalized as the equatorial thermosphere anomaly (ETA), is an anomalous TNW phenomenon occurring at the dip equator because of the latitudinal variations in winds and temperature influenced by the EIA. Evidence of the ETWA was first provided by Raghavarao et al. (1991) through the analysis of ionospheric and neutral measurements obtained with the WATS and Langmuir Probe aboard the DE-2 satellite (Hoffman and Schmerling, 1982). The authors noted peak zonal winds and minimum temperatures near the dip equator, as well as a sudden reduction in wind velocity by ~100 m/s on either side of the equator; both observations correlated well with EIA intensities (Raghavarao and Suhasini, 2002). At low latitudes, the pressure gradient at the EIA crests was significant compared with solar diurnal tides, as highlighted in recent studies (e.g., Hossain et al., 2023). Earlier theories explaining these enhanced temperatures and slower zonal winds at the EIA crests have included excess ion drag (Hedin and Mayr, 1973) and chemical heating from enhanced recombination (Fuller-Rowell et al., 1997). Pant and Sridharan (2001) linked the ETWA to both mechanisms after density and temperature simulations made with derived composition values of ions and molecular oxygen, run using the MSIS-86 model, were found to have failed in capturing the phenomena. However, the absence of simultaneous measurements onboard the DE-2 leaves the theory of chemical heating unconfirmed owing to a lack of observational data. Additionally, Lei JH et al. (2012a), in a study assessing the contribution of these mechanisms through TIEGCM simulations, concluded that chemical heating alone was insufficient to explain ETA crests, with more recent theories (Maruyama et al., 2003; Lei JH et al., 2012b, 2014) suggesting field-aligned ion drag from increased plasma density over the EIA crests as a key factor. This conclusion was further supported by Hsu et al. (2014), who found that incorporating field-aligned ion drag into the TIEGCM model allowed for the simulation of key ETA features. Coming investigations should focus on further numerical modeling and empirical observations,

such as those from the CHAMP satellite, which will be instrumental in providing clarity on ETWA and ETA mechanisms and dynamics.

Another phenomenon unique to sectors near the dip equator is the occurrence of equatorial plasma bubbles (EPBs), also known as equatorial spread F (ESF), which are large-scale structures characterized by regions of plasma depletion originating from the bottomside F layer during post-sunset hours. The plasma instability growth is dependent on various precursor conditions, including the evening PRE, wave structure, and F layer density gradient (Abdu, 2019). Through the analysis of equatorial electrodynamics, Rishbeth (1971) discovered that zonal winds in the low-latitude F region ionosphere induce nearly vertical polarization electric fields, which in turn drive eastward plasma drift closely aligned with neutral winds. Consequently, the eastward wind-driven Pedersen currents at the sunset terminator causes an upwelling of the F region, which pushes ionospheric plasma upward, causing a perturbation of plasma density. This process leads to bubble formation as a result of Rayleigh–Taylor instability (Farley et al., 1986). This bubble formation can be seen in a study by Sarudin et al. (2021), where the presence of EPBs corresponded to stronger zonal winds. This finding was further supported by a similar investigation by Heelis et al. (2012), in which a reversal in zonal winds caused an uplift in the F region. Moreover, the characteristics of EPBs have been found to vary with changes in TNWs. For instance, Aa et al. (2024) observed enhanced bubble intensity as a result of zonal wind modulation by planetary waves, whereas unique C-shaped EPBs have been identified by Kil et al. (2009) and Woodman and La Hoz (1976) resulting from an eastward tilt caused by strong westward zonal winds in the lower F region (Karan et al., 2023). Conversely, meridional winds have been observed to negatively correlate with the development of EPBs by reducing the evening pre-reversal zonal electric field enhancement and directly suppressing bubble growth (Abdu et al., 2006). Meridional winds have also been suggested to cause EPB displacement in the direction of the wind (Barros et al., 2022). Both components of TNWs substantially influence the development of EPB phenomena in the low-latitude ionosphere. Therefore, more precise prediction models of TNW circulation could enhance the forecasting of EPB events.

4. Conclusions

The study of TNWs over the magnetic equator has illuminated the intricate processes that govern Earth's upper atmosphere. Recent research has unraveled the complex interplay of various physical processes, including the influence of solar activity, magnetospheric processes, geomagnetic forces, and ionospheric responses. These factors collectively shape the dynamic and nonlinear responses in neutral wind patterns, which play a critical role in shaping the dynamics of several key ionospheric phenomena unique to the low-latitude regions. The EEJ, EIA, ETWA, and ionospheric scintillation phenomena are all strongly influenced by TNWs through mechanisms such as ion-neutral interactions, plasma drifts, and wind-induced electric fields. Thermospheric neutral winds modulate the structure, strength, and spatial distribution of these phenomena, often in conjunction with other atmospheric and space weather factors.

The research gaps in understanding equatorial TNWs as discussed in this review highlight several notable limitations. The challenge of measuring TNWs comprehensively, especially over the equator, arises because of the limitations of individual observational techniques. To bridge these data gaps, a combination of ground-based and space-based measurements, supplemented with simulations, is necessary to fully capture the climatology of TNWs and their impacts on the upper atmosphere. Furthermore, establishing a global network of TNW measurement instruments is a promising solution, but it requires international collaboration and coordination. Projects such as SEALION offer a model for expanding data coverage along the magnetic equator. Such networks would benefit from joint funding and shared use of instruments by governments, research institutions, and space agencies. However, this collaborative effort faces technical and logistical challenges, including the calibration and synchronization of instruments, overcoming geographic and political constraints, and addressing issues such as fast data transfers, data latency, and robustness in remote regions. Additional concerns include adverse weather conditions, maintaining a resilient infrastructure, and handling large datasets, all of which require advanced computing resources and robust data security protocols.

The development and deployment of advanced instruments are also crucial for accurate TNW measurements, whereas existing ground-based instrumentation techniques need optimization and improvement. New and existing instruments also require validation and comparison to ensure accuracy and reliability in equatorial TNW research. On the other hand, empirical models are subject to data sparseness at certain altitudes and time ranges because they rely heavily on mid- to high-latitude data, whereas first-principle models face challenges in correlating with observational data and exhibit discrepancies in multiple parameters. Newer models need further validation and comparison with observational data to confirm their effectiveness. Enhanced integration of diverse observational data into both empirical and first-principle models is crucial for better simulation accuracy. Addressing these gaps requires improved model development, better integration of observational data, and improved validation efforts, which will improve our current understanding of the underlying physical processes behind the interplay of space weather phenomena occurring in the equatorial region. Additionally, ML techniques are being explored to enhance TNW forecasting, although challenges remain because of the limited availability of high-resolution datasets.

Future research will aim to untangle the intricate feedback loops among the ionosphere, magnetosphere, and thermosphere, examining how these interactions shape TNW patterns. This comprehensive approach promises to improve predictive models and provide deeper insights into the dynamics of Earth's upper atmosphere. Such studies will have far-reaching implications, not only for space weather but also for broader atmospheric circulation. As scientists continue to explore the complexities near the magnetic equator, their work may reveal a fuller understanding of the forces that drive TNWs and their global effects.

Acknowledgments

Siti Syazwani Nasuha thanks the Ministry of Higher Education

(KPT) Malaysia for the MyBrainSc program. Idahwati Sarudin was supported by Universiti Sains Malaysia through a Short-Term Grant (Project No. 304/PFIZIK/6315730). Nurul Shazana Abdul Hamid received funding from Universiti Kebangsaan Malaysia for funding this work through a University Research Grant (Grant No. GUP-2023-048). We also thank the International Association of Geomagnetism and Aeronomy (IAGA) for the IGRF model (https://www.ncei.noaa.gov/products/international-geomagnetic-reference-field) and the National Oceanic and Atmospheric Administration (NOAA) for the CTIPe model (https://www.swpc.noaa.gov/products/ctipe-total-electron-content-forecast).

References

Aa, E., Pedatella, N. M., and Liu, G. P. (2024). Impacts of the sudden stratospheric warming on equatorial plasma bubbles: Suppression of EPBs and quasi-6-day oscillations. *Remote Sens.*, *16*(8), 1469. https://doi.org/10.3390/rs16081469

Abadi, P., Otsuka, Y., Liu, H. X., Hozumi, K., Martinigrum, D. R., Jamjareegulgarn, P., Thanh, L. T., and Otadoy, R. (2021). Roles of thermospheric neutral wind and equatorial electrojet in pre-reversal enhancement, deduced from observations in Southeast Asia. *Earth Planet. Phys.*, *5*(5), 387–396. https://doi.org/10.26464/epp2021049

Abdu, M. A., Iyer, K. N., de Medeiros, R. T., Batista, I. S., and Sobral, J. H. A. (2006). Thermospheric meridional wind control of equatorial spread F and evening prereversal electric field. *Geophys. Res. Lett.*, *33*(7), L07106. https://doi.org/10.1029/2005GL024835

Abdu, M. A., Batista, I. S., Reinisch, B. W., De Souza, J. R., Sobral, J. H. A., Pedersen, T. R., Medeiros, A. F., Schuch, N. J., De Paula, E. R., and Groves, K. M. (2009). Conjugate Point Equatorial Experiment (COPEX) campaign in Brazil: Electrodynamics highlights on spread *F* development conditions and day-to-day variability. *J. Geophys. Res.: Space Phys.*, *114*(A4), A04308. https://doi.org/10.1029/2008JA013749

Abdu, M. A. (2019). Day-to-day and short-term variabilities in the equatorial plasma bubble/spread F irregularity seeding and development. *Prog. Earth Planet. Sci.*, *6*(1), 11. https://doi.org/10.1186/s40645-019-0258-1

Alken, P., Thébault, E., Beggan, C. D., Amit, H., Aubert, J., Baerenzung, J., Bondar, T. N., Brown, W. J., Califf, S., … Zhou, B. (2021). International geomagnetic reference field: The thirteenth generation. *Earth, Planets Space, 73*(1), 49. https://doi.org/10.1186/s40623-020-01288-x

Ambili, K. M., and Choudhary, R. K. (2022). On the impact of meridional wind circulation changes in the electron density distribution over the Indian equatorial and low latitude ionospheric region during a severe geomagnetic storm. *Adv. Space Res.*, *70*(7), 2058–2069. https://doi.org/10.1016/j.asr.2022.06.027

Anandarao, B. G., and Raghavarao, R. (1979). Gravity waves and tidal winds in the equatorial thermosphere. In M. J. Rycroft (Ed.), *COSPAR: Space Research* (pp. 263–266). Oxford, UK: Pergamon. https://doi.org/10.1016/B978-0-08-023417-5.50046-6

Aruliah, A. L., Griffin, E. M., Yiu, H. C. I., McWhirter, I., and Charalambous, A. (2010). SCANDI—An all-sky Doppler imager for studies of thermospheric spatial structure. *Ann. Geophys.*, *28*(2), 549–567. https://doi.org/10.5194/angeo-28-549-2010

Balan, N., Liu, L. B., and Le, H. J. (2018). A brief review of equatorial ionization anomaly and ionospheric irregularities. *Earth Planet. Phys.*, *2*(4), 257–275. https://doi.org/10.26464/epp2018025

Balthazor, R. L., and Moffett, R. J. (1997). A study of atmospheric gravity waves and travelling ionospheric disturbances at equatorial latitudes. *Ann. Geophys.*, *15*(8), 1048–1056. https://doi.org/10.1007/s00585-997-1048-4

Barros, D., Takahashi, H., Wrasse, C. M., Carrasco, A. J., Figueiredo, C. A. O. B., and Inoue Junior, M. H. (2022). Asymmetric development of equatorial plasma bubbles observed at geomagnetically conjugate points over the Brazilian sector. *J. Geophys. Res.: Space Phys.*, *127*(6), e2021JA030250. https://doi.org/10.1029/2021JA030250

Batista, P. P., Takahashi, H., Gobbi, D., and Medeiros, A. F. (2000). First airglow all sky images at 23°S. *Adv. Space Res.*, *26*(6), 925–928. https://doi.org/10.1016/S0273-1177(00)00031-4

Bello, S. A., Shazana, N., Hamid, A., Abdullah, M., Yoshikawa, A., Hozumi, K., and Tsugawa, T. (2021). Equatorial Electrojet and electron density over Southeast Asian Region during moderate solar activity condition. *Indian J. Radio Space Phys.*, *50*, 125–131. http://wdc.ku

Bittencourt, J. A., and Sahai, Y. (1978). *F*-region neutral winds from ionosonde measurements of h_mF_2 at low latitude magnetic conjugate regions. *J. Atmos. Terr. Phys.*, *40*(6), 669–676. https://doi.org/10.1016/0021-9169(78)90124-1

Blanc, M., and Richmond, A. D. (1980). The ionospheric disturbance dynamo. *J. Geophys. Res.: Space Phys.*, *85*(A4), 1669–1686. https://doi.org/10.1029/ja085ia04p01669

Burns, A. G., Killeen, T. L., Deng, W., Carignan, G. R., and Roble, R. G. (1995). Geomagnetic storm effects in the low-to middle-latitude upper thermosphere. *J. Geophys. Res.: Space Phys.*, *100*(A8), 14673–14691. https://doi.org/10.1029/94ja03232

Burns, A. G., Wang, W. B., and Qian, L. Y. (2021). Neutral composition in the upper atmosphere. In W. B. Wang, et al. (Eds.), *Upper Atmosphere Dynamics and Energetics* (pp. 105–113). Hoboken, New Jersey: Wiley-American Geophysical Union. https://doi.org/10.1002/9781119815631.ch6

Cai, X. G., Burns, A. G., Wang, W. B., Qian, L. Y., Solomon, S. C., Eastes, R. W., McClintock, W. E., and Laskar, F. I. (2021). Investigation of a neutral "tongue" observed by GOLD during the geomagnetic storm on May 11, 2019. *J. Geophys. Res.: Space Phys.*, *126*(6), e2020JA028817. https://doi.org/10.1029/2020JA028817

Cai, Y. H., Yue, X. A., Wang, W. B., Zhang, S. R., Liu, L. B., Liu, H. X., and Wan, W. X. (2019). Long-term trend of topside ionospheric electron density derived from DMSP data during 1995–2017. *J. Geophys. Res.: Space Phys., 124*(12), 10708–10727. https://doi.org/10.1029/2019ja027522

Camporeale, E. (2019). The challenge of machine learning in space weather: Nowcasting and forecasting. *Space Wea.*, *17*(8), 1166–1207. https://doi.org/10.1029/2018sw002061

Chen, G., Zhao, Z. Y., Zhu, G. Q., and Shi, S. Z. (2009). The Wuhan ionospheric sounding systems. *IEEE Geosci. Remote Sens. Lett.*, *6*(4), 748–751. https://doi.org/10.1109/LGRS.2009.2024439

Chen, J. J., and Lei, J. H. (2019). A simulation study on the latitudinal variations of ionospheric zonal electric fields under geomagnetically quiet conditions. *J. Geophys. Res.: Space Phys.*, *124*(2), 1444–1453. https://doi.org/10.1029/2018JA026174

Colerico, M., Mendillo, M., Nottingham, D., Baumgardner, J., Meriwether, J., Mirick, J., Reinisch, B. W., Scali, J. L., Fesen, C. G., and Biondi, M. A. (1996). Coordinated measurements of *F* region dynamics related to the thermospheric midnight temperature maximum. *J. Geophys. Res.: Space Phys.*, *101*(A12), 26783–26793. https://doi.org/10.1029/96JA02337

Colerico, M. J., Mendillo, M., Fesen, C. G., and Meriwether, J. (2006). Comparative investigations of equatorial electrodynamics and low-to-mid latitude coupling of the thermosphere–ionosphere system. *Ann. Geophys.*, *24*(2), 503–513. https://doi.org/10.5194/angeo-24-503-2006

Dandenault, P. B. (2018). MENTAT: A new wind model for Earth's thermosphere. *J. Geophys. Res.: Space Phys.*, *123*(8), 7124–7147. https://doi.org/10.1029/2018JA025551

Davis, C. J., Farmer, A. D., and Aruliah, A. (1995). An optimised method for calculating the O^+–O collision parameter from aeronomical measurements. *Ann. Geophys.*, *13*(5), 541–550. https://doi.org/10.1007/s00585-995-0541-x

De Paula, E. R., Iyer, K. N., Hysell, D. L., Rodrigues, F. S., Kherani, E. A., Jardim, A. C., Rezende, L. F. C., Dutra, S. G., and Trivedi, N. B. (2004). Multi-technique investigations of storm-time ionospheric irregularities over the São Luís equatorial station in Brazil. *Ann. Geophys.*, *22*(10), 3513–3522. https://doi.org/10.5194/angeo-22-3513-2004

Deng, Y., Larsen, M. F., Ridley, A. J., and Zhan, T. Y. (2017). Comparisons of JOULE 1 rocket thermospheric wind observations in high latitudes with GITM simulations. *Sci. China Technol. Sci.*, *60*(3), 412–418. https://doi.org/10.1007/s11431-016-0471-8

Dhadly, M., Sassi, F., Emmert, J., Drob, D., Conde, M., Wu, Q., Makela, J., Budzien, S., and Nicholas, A. (2023). Neutral winds from mesosphere to

thermosphere—Past, present, and future outlook. *Front. Astron. Space Sci.*, *9*, 1050586. https://doi.org/10.3389/fspas.2022.1050586

Dhadly, M. S., Emmert, J. T., Drob, D. P., Conde, M. G., Aruliah, A., Doornbos, E., Shepherd, G. G., Wu, Q., Makela, J. J., … Ridley, A. J. (2019). HL-TWiM empirical model of high-latitude upper thermospheric winds. *J. Geophys. Res.: Space Phys.*, *124*(12), 10592–10618. https://doi.org/10.1029/2019JA027188

Ding, Z. H., Wu, J., Xu, Z. W., Xu, B., and Dai, L. D. (2018). The Qujing incoherent scatter radar: System description and preliminary measurements. *Earth, Planets Space, 70*(1), 87. https://doi.org/10.1186/s40623-018-0859-8

Doornbos, E., Bruinsma, S., Fritsche, B., Visser, P., Van Den IJssel, J., Encarnacao, J. T., and Kern, M. (2013, December). Air Density and Wind Retrieval Using GOCE Data. *ESA Living Planet Symposium, 722*, 7.

Drinkwater, M. R., Haagmans, R., Muzi, D., Popescu, A., Floberghagen, R., Kern, M., and Fehringer, M. (2007). The GOCE gravity mission: ESA's first core Earth explorer. In *Proceedings of the 3rd International GOCE User Workshop* (pp. 1–8). Frascati, Italy: ESA.

Drob, D. P., Emmert, J. T., Crowley, G., Picone, J. M., Shepherd, G. G., Skinner, W., Hays, P., Niciejewski, R. J., Larsen, M., ., … Vincent, R. A. (2008). An empirical model of the Earth's horizontal wind fields: HWM07. *J. Geophys. Res.: Space Phys.*, *113*(A12), A12304. https://doi.org/10.1029/2008JA013668

Drob, D. P., Emmert, J. T., Meriwether, J. W., Makela, J. J., Doornbos, E., Conde, M., Hernandez, G., Noto, J., Zawdie, K. A., … Klenzing, J. H. (2015). An update to the Horizontal Wind Model (HWM): The quiet time thermosphere. *Earth Space Sci.*, *2*(7), 301–319. https://doi.org/10.1002/2014EA000089

Englert, C. R., Babcock, D. D., and Harlander, J. M. (2007). Doppler asymmetric spatial heterodyne spectroscopy (DASH): Concept and experimental demonstration. *Appl. Opt.*, *46*(29), 7297–7307. https://doi.org/10.1364/AO.46.007297

Englert, C. R., Harlander, J. M., Brown, C. M., Meriwether, J. W., Makela, J. J., Castelaz, M., Emmert, J. T., Drob, D. P., and Marr, K. D. (2012). Coincident thermospheric wind measurements using ground-based Doppler Asymmetric Spatial Heterodyne (DASH) and Fabry–Perot Interferometer (FPI) instruments. *J. Atmos. Solar-Terr. Phys.*, *86*, 92–98. https://doi.org/10.1016/j.jastp.2012.07.002

Englert, C. R., Harlander, J. M., Brown, C. M., Marr, K. D., Miller, I. J., Stump, J. E., Hancock, J., Peterson, J. Q., Kumler, J., … Immel, T. J. (2017). Michelson Interferometer for Global High-resolution Thermospheric Imaging (MIGHTI): Instrument design and calibration. *Space Sci. Rev.*, *212*(1-2), 553–584. https://doi.org/10.1007/s11214-017-0358-4

Evans, J. V. (1969). Theory and practice of ionosphere study by Thomson scatter radar. *Proc. IEEE*, *57*(4), 496–530. https://doi.org/10.1109/PROC.1969.7005

Fagundes, P. R., Sahai, Y., Bittencourt, J. A., and Takahashi, H. (1995). Observations of thermospheric neutral winds and temperatures at Cachoeira Paulista (23°S, 45°W) during a geomagnetic storm. *Adv. Space Res.*, *16*(5), 27–30. https://doi.org/10.1016/0273-1177(95)00169-F

Farley, D. T., Bonelli, E., Fejer, B. G., and Larsen, M. F. (1986). The prereversal enhancement of the zonal electric field in the equatorial ionosphere. *J. Geophys. Res.: Space Phys.*, *91*(A12), 13723–13728. https://doi.org/10.1029/ja091ia12p13723

Farley, D. T. (1991). Early incoherent scatter observations at Jicamarca. *J. Atmos. Terr. Phys.*, *53*(8), 665–675. https://doi.org/10.1016/0021-9169(91)90120-V

Farmer, A. D., Winser, K. J., Aruliah, A., and Rees, D. (1990). Ion-neutral dynamics: Comparing Fabry–Perot measurements of neutral winds with those derived from radar observations. *Adv. Space Res.*, *10*(6), 281–286. https://doi.org/10.1016/0273-1177(90)90261-W

Fejer, B. G., Blanc, M., and Richmond, A. D. (2017). Post-storm middle and low-latitude ionospheric electric fields effects. *Space Sci. Rev.*, *206*(1-4), 407–429. https://doi.org/10.1007/s11214-016-0320-x

Fesen, C. G., Hysell, D. L., Meriwether, J. M., Mendillo, M., Fejer, B. G., Roble, R. G., Reinisch, B. W., and Biondi, M. A. (2002). Modeling the low-latitude thermosphere and ionosphere. *J. Atmos. Solar-Terr. Phys.*, *64*(12-14), 1337–1349. https://doi.org/10.1016/S1364-6826(02)00098-6

Florescu-Mitchell, A. I., and Mitchell, J. B. A. (2006). Dissociative recombination. *Phys. Rep.*, *430*(5-6), 277–374. https://doi.org/10.1016/j.physrep.2006.04.002

Forbes, J. M. (1981). The equatorial electrojet. *Rev. Geophys.*, *19*(3), 469–504. https://doi.org/10.1029/RG019i003p00469

Fuller-Rowell, T. J., Codrescu, M. V, Fejer, B. G., Borer, W., Marcos, F., and Anderson, D. N. (1997). Dynamics of the low-latitude thermosphere: Quiet and disturbed conditions. *J. Atmos. Solar-Terr. Phys.*, *59*(13), 1533–1540. https://doi.org/10.1016/S1364-6826(96)00154-X

Gerrard, A. J., and Meriwether, J. W. (2011). Initial daytime and nighttime SOFDI observations of thermospheric winds from Fabry–Perot Doppler shift measurements of the 630-nm OI line-shape profile. *Ann. Geophys.*, *29*(9), 1529–1536. https://doi.org/10.5194/angeo-29-1529-2011

Gordon, W. E. (1958). Incoherent scattering of radio waves by free electrons with applications to space exploration by radar. *Proc. IRE*, *46*(11), 1824–1829. https://doi.org/10.1109/JRPROC.1958.286852

Hamid, N. S. A., Liu, H. X., Uozumi, T., Yumoto, K., Veenadhari, B., Yoshikawa, A., and Sanchez, J. A. (2014). Relationship between the equatorial electrojet and global Sq currents at the dip equator region. *Earth Planets Space*, *66*(1), 146. https://doi.org/10.1186/s40623-014-0146-2

Hamid, N. S. A., Rosli, N. I. M., Ismail, W. N. I., and Yoshikawa, A. (2021). Effects of solar activity on ionospheric current system in the Southeast Asia region. *Indian J. Phys.*, *95*(4), 543–550. https://doi.org/10.1007/s12648-020-01734-2

Hanbaba, R. (1995). Statistical use of ionosonde data for IRI. *Adv. Space Res.*, *15*(2), 17–22. https://doi.org/10.1016/S0273-1177(99)80019-2

Harding, B. J., Makela, J. J., Qin, J. Q., Fisher, D. J., Martinis, C. R., Noto, J., and Wrasse, C. M. (2017a). Atmospheric scattering effects on ground-based measurements of thermospheric vertical wind, horizontal wind, and temperature. *J. Geophys. Res.: Space Phys.*, *122*(7), 7654–7669. https://doi.org/10.1002/2017JA023942

Harding, B. J., Makela, J. J., Englert, C. R., Marr, K. D., Harlander, J. M., England, S. L., and Immel, T. J. (2017b). The MIGHTI wind retrieval algorithm: Description and verification. *Space Sci. Rev.*, *212*(1-2), 585–600. https://doi.org/10.1007/s11214-017-0359-3

Harding, B. J., Ridley, A. J., and Makela, J. J. (2019). Thermospheric weather as observed by ground-based FPIs and modeled by GITM. *J. Geophys. Res.: Space Phys.*, *124*(2), 1307–1316. https://doi.org/10.1029/2018JA026032

Hari, S. S., and Krishna Murthy, B. V. (1995). Seasonal variations of equatorial night-time thermospheric meridional winds. *J. Atmos. Terr. Phys.*, *57*(11), 1241–1246. https://doi.org/10.1016/0021-9169(95)00007-O

Haridas, M. K., Manju, G., and Arunamani, T. (2016). Solar activity variations of nocturnal thermospheric meridional winds over Indian longitude sector. *J. Atmos. Solar-Terr. Phys.*, *147*, 21–27. https://doi.org/10.1016/j.jastp.2016.06.010

Harper, R. (1973). Nighttime meridional neutral winds near 350 km at low to mid-latitudes. *Journal of Atmospheric and Terrestrial Physics*, *35*(11), 2023–2034. https://doi.org/10.1016/0021-9169(73)90116-5

Hays, P. B., Killeen, T. L., and Kennedy, B. C. (1981). The Fabry–Perot interferometer on dynamics explorer. *Space Sci. Instrum.*, *5*, 395–416.

Hedin, A. E., and Mayr, H. G. (1973). Magnetic control of the near equatorial neutral thermosphere. *J. Geophys. Res.: Space Phys.*, *78*(10), 1688–1691. https://doi.org/10.1029/ja078i010p01688

Hedin, A. E. (1987). MSIS-86 thermospheric model. *J. Geophys. Res.: Space Phys.*, *92*(A5), 4649–4662. https://doi.org/10.1029/ja092ia05p04649

Heelis, R. A., Crowley, G., Rodrigues, F., Reynolds, A., Wilder, R., Azeem, I., and Maute, A. (2012). The role of zonal winds in the production of a pre-reversal enhancement in the vertical ion drift in the low latitude ionosphere. *J. Geophys. Res.: Space Phys.*, *117*(A8), A08308. https://doi.org/10.1029/2012JA017547

Heelis, R. A., and Maute, A. (2020). Challenges to understanding the Earth's ionosphere and thermosphere. *J. Geophys. Res.: Space Phys.*, *125*(7), e2019JA027497. https://doi.org/10.1029/2019JA027497

Heppner, J. P., and Miller, M. L. (1982). Thermospheric winds at high latitudes from chemical release observations. *J. Geophys. Res.: Space Phys.*, *87*(A3), 1633–1647. https://doi.org/10.1029/ja087ia03p01633

Herrero, F. A., Mayr, H. G., and Spencer, N. W. (1988). Low latitude thermospheric meridional winds between 250 and 450 km altitude: AE-E

satellite data. *J. Atmos. Terr. Phys.*, *50*(10–11), 1001–1006. https://doi.org/10.1016/0021-9169(88)90087-6

Hines, C. O. (1960). Internal atmospheric gravity waves at ionospheric heights. *Can. J. Phys.*, *38*(11), 1441–1481. https://doi.org/10.1139/p60-150

Hoffman, R. A., and Schmerling, E. R. (1982). Dynamics explorer program: An overview. *Space Science Instrumentation, 5*, 345–348.

Hosokawa, K., Takami, K., Saito, S., Ogawa, Y., Otsuka, Y., Shiokawa, K., Chen, C. H., and Lin, C. H. (2020). Observations of equatorial plasma bubbles using a low-cost 630.0-nm all-sky imager in Ishigaki Island, Japan. *Earth Planets Space*, *72*(1), 56. https://doi.org/10.1186/s40623-020-01187-1

Hossain, M., Pant, T. K., and Vineeth, C. (2023). Nocturnal thermospheric neutral wind and temperature measurement using a Fabry–Perot Interferometer: First results from an equatorial Indian station. *Adv. Space Res.*, *72*(2), 598–613. https://doi.org/10.1016/j.asr.2023.03.040

Hsu, V. W., Thayer, J. P., Lei, J. H., and Wang, W. B. (2014). Formation of the equatorial thermosphere anomaly trough: Local time and solar cycle variations. *J. Geophys. Res.: Space Phys.*, *119*(12), 10456–10473. https://doi.org/10.1002/2014JA020416

Immel, T. J., England, S. L., Mende, S. B., Heelis, R. A., Englert, C. R., Edelstein, J., Frey, H. U., Korpela, E. J., Taylor, E. R., … Sirk, M. M. (2018). The ionospheric connection explorer mission: Mission goals and design. *Space Sci. Rev.*, *214*(1), 13. https://doi.org/10.1007/s11214-017-0449-2

Jiang, G. Y., Xu, J. Y., Wang, W. B., Yuan, W., Zhang, S. R., Yu, T., Zhang, X. X., Huang, C., Kerr, R. B., … Li, Q. Z. (2018). A comparison of quiet time thermospheric winds between FPI observations and model calculations. *J. Geophys. Res.: Space Phys.*, *123*(9), 7789–7805. https://doi.org/10.1029/2018JA025424

Kalita, B. R., Hazarika, R., Kakoti, G., Bhuyan, P. K., Chakrabarty, D., Seemala, G. K., Wang, K., Sharma, S., Yokoyama, T., … Roy, P. (2016). Conjugate hemisphere ionospheric response to the St. Patrick's day storms of 2013 and 2015 in the 100°E longitude sector. *J. Geophys. Res.: Space Phys.*, *121*(11), 11364–11390. https://doi.org/10.1002/2016JA023119

Karan, D. K., Eastes, R. W., Martinis, C. R., Daniell, R. E., Solomon, S. C., and McClintock, W. E. (2023). Unique combinations of differently shaped equatorial plasma bubbles occurring within a small longitude range. *J. Geophys. Res.: Space Phys.*, *128*(11), e2023JA031625. https://doi.org/10.1029/2023JA031625

Ke, K. J., Su, C. L., Kuong, R. M., Chen, H. C., Lin, H. S., Chiu, P. H., Ko, C. Y., and Chu, Y. H. (2022). New Chung-Li ionosonde in Taiwan: System description and preliminary results. *Remote Sens.*, *14*(8), 1913. https://doi.org/10.3390/rs14081913

Khadka, S. M., Valladares, C. E., Sheehan, R., and Gerrard, A. J. (2018). Effects of electric field and neutral wind on the asymmetry of equatorial ionization anomaly. *Radio Sci.*, *53*(5), 683–697. https://doi.org/10.1029/2017RS006428

Kil, H., Heelis, R. A., Paxton, L. J., and Oh, S. J. (2009). Formation of a plasma depletion shell in the equatorial ionosphere. *J. Geophys. Res.: Space Phys.*, *114*(A11), A11302. https://doi.org/10.1029/2009JA014369

Killeen, T. L., and Roble, R. G. (1988). Thermosphere dynamics: Contributions from the first 5 years of the dynamics explorer program. *Rev. Geophys.*, *26*(2), 329–367. https://doi.org/10.1029/RG026i002p00329

Kofman, W., Lathuillere, C., and Pibaret, B. (1986). Neutral atmosphere studies in the altitude range 90–110 km using EISCAT. *J. Atmos. Terr. Phys.*, *48*(9-10), 837–847. https://doi.org/10.1016/0021-9169(86)90058-9

Larsen, M. F., and Odom, C. D. (1997). Observations of altitudinal and latitudinal E-region neutral wind gradients near sunset at the magnetic equator. *Geophys. Res. Lett.*, *24*(13), 1711–1714. https://doi.org/10.1029/97GL01469

Larsen, M. F. (2002). Winds and shears in the mesosphere and lower thermosphere: Results from four decades of chemical release wind measurements. *J. Geophys. Res.: Space Phys.*, *107*(A8), 1215. https://doi.org/10.1029/2001JA000218

Laštovička, J. (2023). Progress in investigating long-term trends in the mesosphere, thermosphere, and ionosphere. *Atmos. Chem. Phys.*, *23*(10), 5783–5800. https://doi.org/10.5194/acp-23-5783-2023

Le, G., Liu, G., Yizengaw, E., and Englert, C. R. (2022). Intense equatorial electrojet and counter electrojet caused by the 15 January 2022 Tonga volcanic eruption: Space-and ground-based observations. *Geophysical Research Letters*, *49*(11). https://doi.org/10.1029/2022gl099002

Lei, J. H., Thayer, J. P., Wang, W. B., Luan, X. L., Dou, X. K., and Roble, R. (2012a). Simulations of the equatorial thermosphere anomaly: Physical mechanisms for crest formation. *J. Geophys. Res.: Space Phys.*, *117*(A6), A06318. https://doi.org/10.1029/2012JA017613

Lei, J. H., Thayer, J. P., Wang, W. B., Richmond, A. D., Roble, R., Luan, X. L., Dou, X. K., Xue, X. H., and Li, T. (2012b). Simulations of the equatorial thermosphere anomaly: Field-aligned ion drag effect. *J. Geophys. Res.: Space Phys.*, *117*(A1), A01304. https://doi.org/10.1029/2011JA017114

Lei, J. H., Wang, W. B., Thayer, J. P., Luan, X. L., Dou, X. K., Burns, A. G., and Solomon, S. C. (2014). Simulations of the equatorial thermosphere anomaly: Geomagnetic activity modulation. *J. Geophys. Res.: Space Phys.*, *119*(8), 6821–6832. https://doi.org/10.1002/2014ja020152

Liu, H. L., Foster, B. T., Hagan, M. E., McInerney, J. M., Maute, A., Qian, L., Richmond, A. D., Roble, R. G., Solomon, S. C., … Oberheide, J. (2010). Thermosphere extension of the whole atmosphere community climate model. *J. Geophys. Res.: Space Phys.*, *115*(A12), A12302. https://doi.org/10.1029/2010JA015586

Liu, H. L., Bardeen, C. G., Foster, B. T., Lauritzen, P., Liu, J., Lu, G., Marsh, D. R., Maute, A., McInerney, J. M., … Wang, W. B. (2018). Development and validation of the whole atmosphere community climate model with thermosphere and ionosphere extension (WACCM-X 2.0). *J. Adv. Model. Earth Syst.*, *10*(2), 381–402. https://doi.org/10.1002/2017MS001232

Liu, H. L., Wang, W., Huba, J. D., Lauritzen, P. H., and Vitt, F. (2023). Atmospheric and ionospheric responses to Hunga-Tonga volcano eruption simulated by WACCM-X. *Geophys. Res. Lett.*, *50*(10), e2023GL103682. https://doi.org/10.1029/2023GL103682

Liu, H. X., Doornbos, E., and Nakashima, J. (2016). Thermospheric wind observed by GOCE: Wind jets and seasonal variations. *J. Geophys. Res.: Space Phys.*, *121*(7), 6901–6913. https://doi.org/10.1002/2016JA022938

Liu, J. Y., Rajesh, P. K., Liao, Y. A., Chum, J., Kan, K. W., and Lee, I. T. (2024). Airglow observed by a full-band imager together with multi-instruments in Taiwan during nighttime of 1 November 2021. *Adv. Space Res.*, *73*(1), 663–671. https://doi.org/10.1016/j.asr.2023.09.013

Liu, Z. L., Barlow, J. F., Chan, P. W., Fung, J. C. H., Li, Y. G., Ren, C., Mak, H. W. L., and Ng, E. (2019). A review of progress and applications of pulsed Doppler wind LiDARs. *Remote Sens.*, *11*(21), 2522. https://doi.org/10.3390/rs11212522

Lu, G., Richmond, A. D., Lühr, H., and Paxton, L. (2016). High-latitude energy input and its impact on the thermosphere. *J. Geophys. Res.: Space Phys.*, *121*(7), 7108–7124. https://doi.org/10.1002/2015JA022294

Lynn, K. J. W., Harris, T. J., and Sjarifudin, M. (2006). Relationships between electron density, height and sub-peak ionospheric thickness in the night equatorial ionosphere. *Ann. Geophys.*, *24*(5), 1343–1353. https://doi.org/10.5194/angeo-24-1343-2006

Makela, J. J., Meriwether, J. W., Lima, J. P., Miller, E. S., and Armstrong, S. J. (2009). The remote equatorial nighttime observatory of ionospheric regions project and the international heliospherical year. *Earth Moon Planets*, *104*(1-4), 211–226. https://doi.org/10.1007/s11038-008-9289-0

Makela, J. J., Meriwether, J. W., Huang, Y. Y., and Sherwood, P. J. (2011). Simulation and analysis of a multi-order imaging Fabry–Perot interferometer for the study of thermospheric winds and temperatures. *Appl. Opt.*, *50*(22), 4403–4416. https://doi.org/10.1364/AO.50.004403

Makela, J. J., Fisher, D. J., Meriwether, J. W., Buriti, R. A., and Medeiros, A. F. (2013). Near-continual ground-based nighttime observations of thermospheric neutral winds and temperatures over equatorial Brazil from 2009 to 2012. *J. Atmos. Solar-Terr. Phys.*, *103*, 94–102. https://doi.org/10.1016/j.jastp.2012.11.019

Marr, K. D., Englert, C. R., and Harlander, J. M. (2012). Flat-fields in DASH interferometry. *Opt. Express*, *20*(9), 9535–9544. https://doi.org/10.1364/OE.20.009535

Marsal, S., Richmond, A. D., Maute, A., and Anderson, B. J. (2012). Forcing the TIEGCM model with Birkeland currents from the active magnetosphere and planetary electrodynamics response experiment. *J. Geophys. Res.: Space Phys.*, *117*(A6), A06308. https://doi.org/10.1029/2011JA017416

Martinis, C., Meriwether, J., Niciejewski, R., Biondi, M., Fesen, C., and Mendillo, M.

(2001). Zonal neutral winds at equatorial and low latitudes. *J. Atmos. Solar-Terr. Phys.*, *63*(14), 1559–1569. https://doi.org/10.1016/S1364-6826(01)00022-0

Martinis, C., Eccles, J. V., Baumgardner, J., Manzano, J., and Mendillo, M. (2003). Latitude dependence of zonal plasma drifts obtained from dual-site airglow observations. *J. Geophys. Res.: Space Phys.*, *108*(A3), 1129. https://doi.org/10.1029/2002JA009462

Martinis, C., Baumgardner, J., Smith, S. M., Colerico, M., and Mendillo, M. (2006). Imaging science at El Leoncito, Argentina. *Ann. Geophys.*, *24*(5), 1375–1385. https://doi.org/10.5194/angeo-24-1375-2006

Maruyama, N., Watanabe, S., and Fuller-Rowell, T. J. (2003). Dynamic and energetic coupling in the equatorial ionosphere and thermosphere. *J. Geophys. Res.: Space Phys.*, *108*(A11), 1396. https://doi.org/10.1029/2002JA009599

Maruyama, T., Nozaki, K., Yamamoto, M., and Fukao, S. (2002). Ionospheric height changes at two closely separated equatorial stations and implications in spread *F* onsets. *J. Atmos. Solar-Terr. Phys.*, *64*(12-14), 1557–1563. https://doi.org/10.1016/S1364-6826(02)00093-7

Maruyama, T., Ma, G. Y., and Nakamura, M. (2004). Signature of TEC storm on 6 November 2001 derived from dense GPS receiver network and ionosonde chain over Japan. *J. Geophys. Res.: Space Phys.*, *109*(A10), A10302. https://doi.org/10.1029/2004JA010451

Maruyama, T., Kawamura, M., Saito, S., Nozaki, K., Kato, H., Hemmakorn, N., Boonchuk, T., Komolmis, T., and Ha Duyen, C. (2007). Low latitude ionosphere–thermosphere dynamics studies with ionosonde chain in Southeast Asia. *Ann. Geophys.*, *25*(7), 1569–1577. https://doi.org/10.5194/angeo-25-1569-2007

Maruyama, T., Saito, S., Kawamura, M., and Nozaki, K. (2008). Thermospheric meridional winds as deduced from ionosonde chain at low and equatorial latitudes and their connection with midnight temperature maximum. *Journal of Geophysical Research Atmospheres*, *113*(A9). https://doi.org/10.1029/2008ja013031

McHugh, M., Fritts, D., and Gordley, L. (2014). The Doppler wind and temperature sounder. In *The 13th Biennial HITRAN Conference (HITRAN13)*. Cambridge, Massachusetts: Harvard-Smithsonian Center for Astrophysics. https://doi.org/10.5281/ZENODO.11111

McNamara, L. F., and Wilkinson, P. J. (2009). Spatial correlations of f_0F_2 deviations and their implications for global ionospheric models: 1. Ionosondes in Australia and Papua New Guinea. *Radio Sci.*, *44*(2), RS2016. https://doi.org/10.1029/2008rs003955

Medeiros, A. F., Buriti, R. A., Machado, E. A., Takahashi, H., Batista, P. P., Gobbi, D., and Taylor, M. J. (2004). Comparison of gravity wave activity observed by airglow imaging at two different latitudes in Brazil. *J. Atmos. Solar-Terr. Phys.*, *66*(6-9), 647–654. https://doi.org/10.1016/j.jastp.2004.01.016

Mendillo, M., Baumgardner, J., Martinis, C., and Wroten, J. (2015). North-South America Network of Magnetically Conjugate All-Sky Imagers (DTIC_ADA616484). Trustees of Boston University. https://apps.dtic.mil/sti/tr/pdf/ADA616484.pdf

Meriwether, Jr. J. W., Moody, J. W., Biondi, M. A., and Roble, R. G. (1986). Optical interferometric measurements of nighttime equatorial thermospheric winds at Arequipa, Peru. *J. Geophys. Res.: Space Phys.*, *91*(A5), 5557–5566. https://doi.org/10.1029/ja091ia05p05557

Miller, K. L., Torr, D. G., and Richards, P. G. (1986). Meridional winds in the thermosphere derived from measurement of F_2 layer height. *J. Geophys. Res.: Space Phys.*, *91*(A4), 4531–4535. https://doi.org/10.1029/ja091ia04p04531

Millward, G. H., Müller-Wodarg, I. C. F., Aylward, A. D., Fuller-Rowell, T. J., Richmond, A. D., and Moffett, R. J. (2001). An investigation into the influence of tidal forcing on F region equatorial vertical ion drift using a global ionosphere–thermosphere model with coupled electrodynamics. *J. Geophys. Res.: Space Phys.*, *106*(A11), 24733–24744. https://doi.org/10.1029/2000ja000342

Murty, G. S. N., and Kim, J. S. (1988). Thermospheric temperatures and meridional winds measured at Albany, New York during geomagnetically disturbed periods. *Planet. Space Sci.*, *36*(7), 677–685. https://doi.org/10.1016/0032-0633(88)90116-X

Navarro, L. A., and Fejer, B. G. (2019). Storm-time thermospheric winds over Peru. *J. Geophys. Res.: Space Phys.*, *124*(12), 10415–10427. https://doi.org/10.1029/2019JA027256

Navarro, L. A., and Fejer, B. G. (2020). Storm-time coupling of equatorial nighttime *F* region neutral winds and plasma drifts. *J. Geophys. Res.: Space Phys.*, *125*(9), e2020JA028253. https://doi.org/10.1029/2020JA028253

Niranjan, K., Brahmanandam, P. S., and Srivani, B. (2006). Signatures of equatorial midnight temperature maximum as observed from in situ and ground-based ionospheric measurements in the Indian sector. *Journal of Geophysical Research Atmospheres*, *111*(A7). https://doi.org/10.1029/2005ja011386

Okoh, D., Rabiu, B., Shiokawa, K., Otsuka, Y., Segun, B., Falayi, E., Onwuneme, S., and Kaka, R. (2017). First study on the occurrence frequency of equatorial plasma bubbles over West Africa using an all-sky airglow imager and GNSS receivers. *J. Geophys. Res.: Space Phys.*, *122*(12), 12430–12444. https://doi.org/10.1002/2017JA024602

Okoh, D. I., Rabiu, A. B., Shiokawa, K., Otsuka, Y., Wu, Q., Seemala, G. K., and Katamzi-Joseph, Z. T. (2021). An experimental investigation into the possible connections between the zonal neutral wind speeds and equatorial plasma bubble drift velocities over the African equatorial region. *J. Atmos. Solar-Terr. Phys.*, *220*, 105663. https://doi.org/10.1016/j.jastp.2021.105663

Oyama, S. I., Aikio, A., Sakanoi, T., Hosokawa, K., Vanhamäki, H., Cai, L., Virtanen, I., Pedersen, M., Shiokawa, K., … Ogawa, Y. (2023). Geomagnetic activity dependence and dawn–dusk asymmetry of thermospheric winds from 9-year measurements with a Fabry–Perot interferometer in Tromsø, Norway. *Earth Planets Space*, *75*(1), 70. https://doi.org/10.1186/s40623-023-01829-0

Pant, T. K., and Sridharan, R. (2001). Plausible explanation for the equatorial temperature and wind anomaly (ETWA) based on chemical and dynamical processes. *J. Atmos. Solar-Terr. Phys.*, *63*(9), 885–891. https://doi.org/10.1016/S1364-6826(00)00196-6

Paulino, I., Fragoso De Medeiros, A., Buriti, R. A., Takahashi, H., Sobral, J. H. A., and Gobbi, D. (2011). Plasma bubble zonal drift characteristics observed by airglow images over Brazilian tropical region. *Braz. J. Geophys.*, *29*(2), 239–246. https://doi.org/10.1590/S0102-261X2011000200003

Pelz, D. T., Reber, C. A., Hedin, A. E., and Carignan, G. R. (1973). A neutral-atmosphere composition experiment for the Atmosphere Explorer-C, -D, and -E. *Radio Sci.*, *8*(4), 277–285. https://doi.org/10.1029/RS008i004p00277

Pfaff, R., Larsen, M., Abe, T., Habu, H., Clemmons, J., Freudenreich, H., Rowland, D., Bullett, T., Yamamoto, M. Y., … Angelopoulos, V. (2020). Daytime dynamo electrodynamics with spiral currents driven by strong winds revealed by vapor trails and sounding rocket probes. *Geophys. Res. Lett.*, *47*(15), e2020GL088803. https://doi.org/10.1029/2020GL088803

Polekh, N., Zolotukhina, N., Kurkin, V., Zherebtsov, G., Shi, J., Wang, G., and Wang, Z. (2017). Dynamics of ionospheric disturbances during the 17–19 March 2015 geomagnetic storm over East Asia. *Adv. Space Res.*, *60*(11), 2464–2476. https://doi.org/10.1016/j.asr.2017.09.030

Qian, L. Y., Burns, A. G., Wang, W. B., Solomon, S. C., and Zhang, Y. L. (2016). Longitudinal variations of thermospheric composition at the solstices. *J. Geophys. Res.: Space Phys.*, *121*(7), 6818–6829. https://doi.org/10.1002/2016JA022898

Rabiu, A. B., Okoh, D. I., Wu, Q., Bolaji, O. S., Abdulrahim, R. B., Dare-Idowu, O. E., and Obafaye, A. A. (2021). Investigation of the variability of night-time equatorial thermospheric winds over Nigeria, West Africa. *J. Geophys. Res.: Space Phys.*, *126*(3), e2020JA028528. https://doi.org/10.1029/2020JA028528

Raghavarao, R., Wharton, L. E., Spencer, N. W., Mayr, H. G., and Brace, L. H. (1991). An equatorial temperature and wind anomaly (ETWA). *Geophys. Res. Lett.*, *18*(7), 1193–1196. https://doi.org/10.1029/91GL01561

Raghavarao, R., and Suhasini, R. (2002). Equatorial temperature and wind anomaly (ETWA)—A review. *J. Atmos. Solar-Terr. Phys.*, *64*(12-14), 1371–1381. https://doi.org/10.1016/S1364-6826(02)00100-1

Ramsingh Sripathi, R. S., Sreekumar, S., Banola, S., Emperumal, K., Tiwari, P., and Kumar, B. S. (2015). Low-latitude ionosphere response to super geomagnetic storm of 17/18 March 2015: Results from a chain of ground-

based observations over Indian sector. *J. Geophys. Res.: Space Phys.*, *120*(12), 10864–10882. https://doi.org/10.1002/2015JA021509

Reddy, C. A., and Devasia, C. V. (1981). Height and latitude structure of electric fields and currents due to local east–west winds in the equatorial electrojet. *J. Geophys. Res.: Space Phys.*, *86*(A7), 5751–5767. https://doi.org/10.1029/ja086ia07p05751

Reber, C. A., Trevathan, C. E., McNeal, R. J., and Luther, M. R. (1993). The Upper Atmosphere Research Satellite (UARS) mission. *J. Geophys. Res.: Atmos.*, *98*(D6), 10643–10647. https://doi.org/10.1029/92JD02828

Reigber, C., Lühr, H., and Schwintzer, P. (2002). CHAMP mission status. *Adv. Space Res.*, *30*(2), 129–134. https://doi.org/10.1016/S0273-1177(02)00276-4

Reinisch, B. W. (1993). The Digisonde network and databasing. In *Proceedings of the XXIVth General Assembly*. Kyoto: International Union of Radio Science.

Ren, Z. P., Wan, W. X., and Liu, L. B. (2009). GCITEM-IGGCAS: A new global coupled ionosphere–thermosphere–electrodynamics model. *J. Atmos. Solar-Terr. Phys.*, *71*(17-18), 2064–2076. https://doi.org/10.1016/j.jastp.2009.09.015

Ridley, A. J., Deng, Y., and Tóth, G. (2006). The global ionosphere–thermosphere model. *J. Atmos. Solar-Terr. Phys.*, *68*(8), 839–864. https://doi.org/10.1016/j.jastp.2006.01.008

Rishbeth, H. (1971). The *F*-layer dynamo. *Planet. Space Sci.*, *19*(2), 263–267. https://doi.org/10.1016/0032-0633(71)90205-4

Rishbeth, H. (1972). Thermospheric winds and the *F*-region: A review. *J. Atmos. Terr. Phys.*, *34*(1), 1–47. https://doi.org/10.1016/0021-9169(72)90003-7

Rosli, N. I. M., Hamid, N. S. A., Abdullah, M., Yusof, K. A., Yoshikawa, A., Uozumi, T., and Rabiu, B. (2022). The variation of counter-electrojet current at the Southeast Asian sector during different solar activity levels. *Applied Sciences*, *12*(14), 7138. https://doi.org/10.3390/app12147138

Sahai, Y., Aarons, J., Mendillo, M., Baumgardner, J., Bittencourt, J. A., and Takahashi, H. (1994). OI 630 nm imaging observations of equatorial plasma depletions at 16° S dip latitude. *J. Atmos. Terr. Phys.*, *56*(11), 1461–1475. https://doi.org/10.1016/0021-9169(94)90113-9

Salah, J. E., and Holt, J. M. (1974). Midlatitude thermospheric winds from incoherent scatter radar and theory. *Radio Sci.*, *9*(2), 301–313. https://doi.org/10.1029/RS009i002p00301

Sarudin, I., Hamid, N. S. A., Abdullah, M., Buhari, S. M., Shiokawa, K., Otsuka, Y., Hozumi, K., and Jamjareegulgarn, P. (2021). Influence of zonal wind velocity variation on equatorial plasma bubble occurrences over Southeast Asia. *J. Geophys. Res.: Space Phys.*, *126*(5), e2020JA028994. https://doi.org/10.1029/2020JA028994

Sarudin, I., Hamid, N. S. A., Abdullah, M., Syakirah, F. N., Rusli, M., Otsuka, Y., Shiokawa, K., Yatini, C., Komonjinda, S., and Somboon, E. (2022). Variations of zonal wind velocity in the thermosphere observed at Southeast Asian sector during quiet and active geomagnetic days. *J. Fiz. Malays.*, *43*(1), 10009–10017.

Sassi, F., McCormack, J. P., Tate, J. L., Kuhl, D. D., and Baker, N. L. (2021). Assessing the impact of middle atmosphere observations on day-to-day variability in lower thermospheric winds using WACCM-X. *J. Atmos. Solar-Terr. Phys.*, *212*, 105486. https://doi.org/10.1016/j.jastp.2020.105486

Sastri, J. H., Rao, H. N. R., Somayajulu, V. V, and Chandra, H. (1994). Thermospheric meridional neutral winds associated with equatorial midnight temperature maximum (MTM). *Geophys. Res. Lett.*, *21*(9), 825–828. https://doi.org/10.1029/93GL03009

Seba, E. B., Nigussie, M., and Moldwin, M. B. (2022). The role of global thermospheric zonal winds on the variability of equatorial ionospheric irregularities. *J. Atmos. Solar-Terr. Phys., 233–234*, 105873. https://doi.org/10.1016/j.jastp.2022.105873

Shiokawa, K., Otsuka, Y., Oyama, S., Nozawa, S., Satoh, M., Katoh, Y., Hamaguchi, Y., Yamamoto, Y., and Meriwether, J. (2012). Development of low-cost sky-scanning Fabry–Perot interferometers for airglow and auroral studies. *Earth Planets Space*, *64*(11), 1033–1046. https://doi.org/10.5047/eps.2012.05.004

Sivla, W. T., and McCreadie, H. (2014). Mid-latitude thermospheric zonal winds during the equinoxes. *Adv. Space Res.*, *54*(3), 499–508. https://doi.org/10.1016/j.asr.2014.03.014

Sivla, W. T., Ogunjobi, O., and Tesema, F. (2020). Thermospheric winds over Abuja during solar minimum period. *Adv. Space Res.*, *65*(5), 1424–1431. https://doi.org/10.1016/j.asr.2019.11.042

Solomon, S. C., and Roble, R. G. (2015). Thermosphere. In G. R. North, et al. (Eds.), *Encyclopedia of Atmospheric Sciences* (2nd ed., pp. 402–408). Amsterdam: Academic Press. https://doi.org/10.1016/B978-0-12-382225-3.00408-4

Spencer, N. W., Brace, L. H., and Grimes, D. W. (1973). The Atmosphere Explorer spacecraft system. *Radio Sci.*, *8*(4), 267–269. https://doi.org/10.1029/RS008i004p00267

Spencer, N. W., Carignan, G. R., Mayr, H. G., Niemann, H. B., Theis, R. F., and Wharton, L. E. (1979). The midnight temperature maximum in the Earth's equatorial thermosphere. *Geophys. Res. Lett.*, *6*(6), 444–446. https://doi.org/10.1029/GL006i006p00444

Sreekumar, S., and Sripathi, S. (2016). Nighttime thermospheric meridional winds as inferred from ionosonde parameters over Indian region and their plausible effects on plasma irregularities. *Adv. Space Res.*, *58*(1), 92–107. https://doi.org/10.1016/j.asr.2016.04.009

Sun, X. X., Zhou, C., Feng, J., Yang, H. Y., Zhang, Y. Q., Chen, Z., Xu, T., Deng, Z. X., Zhao, Z. Y., … Lan, T. (2024). Research on short-term forecasting model of global atmospheric temperature and wind in the near space based on deep learning. *Atmosphere*, *15*(9), 1069. https://doi.org/10.3390/atmos15091069

Sutton, E. K., Forbes, J. M., and Nerem, R. S. (2005). Global thermospheric neutral density and wind response to the severe 2003 geomagnetic storms from CHAMP accelerometer data. *J. Geophys. Res.: Space Phys.*, *110*(A9), A09S40. https://doi.org/10.1029/2004JA010985

Tesema, F., Mesquita, R., Meriwether, J., Damtie, B., Nigussie, M., Makela, J., Fisher, D., Harding, B., Yizengaw, E., and Sanders, S. (2017). New results on equatorial thermospheric winds and temperatures from Ethiopia, Africa. *Ann. Geophys.*, *35*(2), 333–344. https://doi.org/10.5194/angeo-35-333-2017

Titheridge, J. E. (1995). Winds in the ionosphere—A review. *J. Atmos. Terr. Phys.*, *57*(14), 1681–1714. https://doi.org/10.1016/0021-9169(95)00091-F

Tsuda, T., Yamamoto, M., Hashiguchi, H., Shiokawa, K., Ogawa, Y., Nozawa, S., Miyaoka, H., and Yoshikawa, A. (2016). A proposal on the study of solar–terrestrial coupling processes with atmospheric radars and ground-based observation network. *Radio Sci.*, *51*(9), 1587–1599. https://doi.org/10.1002/2016RS006035

Venkat Ratnam, M., Akhil Raj, S. T., and Qian, L. Y. (2019). Long-term trends in the low-latitude middle atmosphere temperature and winds: Observations and WACCM-X model simulations. *J. Geophys. Res.: Space Phys.*, *124*(8), 7320–7331. https://doi.org/10.1029/2019JA026928

Vila, P., Rees, D., Merrien, P., and Kone, E. (1998). Fabry–Perot interferometer measurements of neutral winds and F2 layer variations at the magnetic equator. *Ann. Geophys.*, *16*(6), 731–737. https://doi.org/10.1007/s00585-998-0731-4

Wang, W. B., Burns, A. G., and Liu, J. (2021). Upper thermospheric winds: Forcing, variability, and effects. In W. B. Wang, et al. (Eds.), *Upper Atmosphere Dynamics and Energetics* (pp. 41–63). Hoboken, New Jersey: Wiley-American Geophysical Union. https://doi.org/10.1002/9781119815631.ch3

Wang, Y. R., and Bai, X. L. (2022). Comparison of Gaussian processes and Neural Networks for thermospheric density predictions during quiet time and geomagnetic storms. In *Proceedings of 2022 AAS/AIAA Astrodynamics Specialist Conference*. https://par.nsf.gov/biblio/10399776

Weng, L. B., Lei, J. H., Zhong, J. H., Dou, X. K., and Fang, H. X. (2020). A machine-learning approach to derive long-term trends of thermospheric density. *Geophys. Res. Lett.*, *47*(6), e2020GL087140. https://doi.org/10.1029/2020gl087140

Wilkinson, P. J., Pulehetoa, S., Cole, D. G., Hyde, M., Neudegg, D., and Paterson, B. (2005). A New South Pacific ionosonde station-Niue. In Proceedings of the 10th International Association of Geomagnetism and Aeronomy Scientific Assembly in Toulouse. https://www.ursi.org/files/CommissionWebsites/INAG/web-66/2005/niue.pdf

Williams, P. J. S. (1989). Observations of atmospheric gravity waves with incoherent scatter radar. *Adv. Space Res.*, *9*(5), 65–72. https://doi.org/10.1016/0273-1177(89)90342-6

Woodman, R. F., and La Hoz, C. (1976). Radar observations of *F* region

equatorial irregularities. *J. Geophys. Res.: Space Phys.*, *81*(31), 5447–5466. https://doi.org/10.1029/JA081i031p05447

Wu, D. L., Yee, J. H., Schlecht, E., Mehdi, I., Siles, J., and Drouin, B. J. (2016). THz limb sounder (TLS) for lower thermospheric wind, oxygen density, and temperature. *J. Geophys. Res.: Space Phys.*, *121*(7), 7301–7315. https://doi.org/10.1002/2015JA022314

Wu, K., Xu, J. Y., Wang, W. B., Sun, L. C., Liu, X., and Yuan, W. (2017). Interesting equatorial plasma bubbles observed by all-sky imagers in the equatorial region of China. *J. Geophys. Res.: Space Phys.*, *122*(10), 10596–10611. https://doi.org/10.1002/2017JA024561

Wu, Q., Killeen, T. L., and Spencer, N. W. (1994). Dynamics Explorer 2 observations of equatorial thermospheric winds and temperatures: Local time and longitudinal dependences. *J. Geophys. Res.: Space Phys.*, *99*(A4), 6277–6288. https://doi.org/10.1029/93ja02521

Wu, Q., Wang, W., Roble, R. G., Häggström, I., and Strømme, A. (2012). First daytime thermospheric wind observation from a balloon-borne Fabry–Perot interferometer over Kiruna (68N). *Geophys. Res. Lett.*, *39*(14), L14104. https://doi.org/10.1029/2012GL052533

Wu, Q. (2016). *Low latitude aeronomy study in Africa* (DTIC_AD1004769). University Corporation for Atmospheric Research. https://apps.dtic.mil/sti/pdfs/AD1004769.pdf

Xu, H. Q. C., Shiokawa, K., Oyama, S. I., and Otsuka, Y. (2019). Thermospheric wind variations observed by a Fabry–Perot interferometer at Tromsø, Norway, at substorm onsets. *Earth Planets Space*, *71*(1), 93. https://doi.org/10.1186/s40623-019-1072-0

Yamazaki, Y., Richmond, A. D., Maute, A., Liu, H., Pedatella, N., and Sassi, F. (2014). On the day-to-day variation of the equatorial electrojet during quiet periods. *J. Geophys. Res.: Space Phys.*, *119*(8), 6966–6980. https://doi.org/10.1002/2014ja020243

Yamazaki, Y., Harding, B. J., Stolle, C., and Matzka, J. (2021). Neutral wind profiles during periods of eastward and westward equatorial electrojet. *Geophys. Res. Lett.*, *48*(11). https://doi.org/10.1029/2021gl093567

Yizengaw, E., Moldwin, M. B., Zesta, E., Biouele, C. M., Damtie, B., Mebrahtu, A., Rabiu, B., Valladares, C. F., and Stoneback, R. (2014). The longitudinal variability of equatorial electrojet and vertical drift velocity in the African and American sectors. *Ann. Geophys.*, *32*(3), 231–238. https://doi.org/10.5194/angeo-32-231-2014

Yue, X. N., Hu, L. H., Wei, Y., Wan, W. X., and Ning, B. Q. (2018). Ionospheric trend over Wuhan during 1947–2017: Comparison between simulation and observation. *J. Geophys. Res.: Space Phys.*, *123*(2), 1396–1409. https://doi.org/10.1002/2017JA024675

Yue, X. N., Wan, W. X., Ning, B. Q., Jin, L., Ding, F., Zhao, B. Q., Zeng, L. Q., Ke, C. H., Deng, X. H., … Liu, F. Y. (2022). Development of the Sanya incoherent scatter radar and preliminary results. *J. Geophys. Res.: Space Phys.*, *127*(8), e2022JA030451. https://doi.org/10.1029/2022JA030451

Zewdie, G. K., Valladares, C., Cohen, M. B., Lary, D. J., Ramani, D., and Tsidu, G. M. (2021). Data-Driven forecasting of low-latitude ionospheric total electron content using the Random Forest and LSTM machine learning methods. *Space Wea.*, *19*(6), e2020SW002639. https://doi.org/10.1029/2020sw002639

Zhang, X. F., Liu, L. B., and Liu, S. T. (2017). Dependence of thermospheric zonal winds on solar flux, geomagnetic activity, and hemisphere as measured by CHAMP. *J. Geophys. Res.: Space Phys.*, *122*(8), 8893–8914. https://doi.org/10.1002/2016JA023715